Eur. Phys. J. C (2009) 62: 293–317
DOI 10.1140/epjc/s10052-009-1053-8

THE EUROPEAN PHYSICAL JOURNAL C

Regular Article - Experimental Physics

Cross-sections of large-angle hadron production in proton- and pion-nucleus interactions I: beryllium nuclei and beam momenta of +8.9 GeV/*c* and −8.0 GeV/*c*

A. Bolshakova[1], I. Boyko[1], G. Chelkov[1], D. Dedovitch[1], A. Elagin[1,2], M. Gostkin[1], S. Grishin[1], A. Guskov[1], Z. Kroumchtein[1], Yu. Nefedov[1], K. Nikolaev[1], A. Zhemchugov[1], F. Dydak[3], J. Wotschack[3,a], A. De Min[4,b], V. Ammosov[5], V. Gapienko[5], V. Koreshev[5], A. Semak[5], Yu. Sviridov[5], E. Usenko[5,6], V. Zaets[5]

[1] Joint Institute for Nuclear Research, Dubna, Russia
[2] *Present address:* Texas A&M University, College Station, USA
[3] CERN, Geneva, Switzerland
[4] Politecnico di Milano and INFN, Sezione di Milano-Bicocca, Milan, Italy
[5] Institute of High Energy Physics, Protvino, Russia
[6] *Present address:* Institute for Nuclear Research RAS, Moscow, Russia

Received: 23 January 2009 / Revised: 16 April 2009 / Published online: 20 May 2009

Abstract We report on double-differential inclusive cross-sections of the production of secondary protons, deuterons, and charged pions and kaons, in the interactions with a 5% λ_{abs} thick stationary beryllium target, of a +8.9 GeV/*c* proton and pion beam, and a −8.0 GeV/*c* pion beam. Results are given for secondary particles with production angles $20^\circ < \theta < 125^\circ$.

PACS 13.85.Ni · 25.40.Qa

1 Introduction

The HARP experiment arose from the realization that the inclusive differential cross-sections of hadron production in the interactions of low-momentum protons with nuclei were known only within a factor of two to three, while more precise cross-sections are in demand for several reasons, notably for the design of the proton driver of a neutrino factory, for the calculation of the atmospheric neutrino flux, for the flux predictions of conventional neutrino beams, and for the modelling of Monte Carlo generators of hadron–nucleus collisions. Consequently, the HARP detector was designed to carry out a programme of systematic and precise measurements of hadron production by protons and pions with momenta from 1.5 to 15 GeV/*c*. It is shown schematically in Fig. 1.

The detector extended longitudinally over 14.7 m and combined a forward spectrometer with a large-angle spectrometer. The latter comprised a cylindrical Time Projection Chamber (TPC) around the target and an array of Resistive Plate Chambers (RPCs) that surrounded the TPC. The purpose of the TPC was track reconstruction and particle identification by $\mathrm{d}E/\mathrm{d}x$. The purpose of the RPCs was to complement the particle identification by time of flight.

The HARP experiment was performed at the CERN Proton Synchrotron in 2001 and 2002 with a set of stationary targets ranging from hydrogen to lead, including beryllium.

We report on the large-angle production (polar angle θ in the range $20^\circ < \theta < 125^\circ$) of secondary protons and charged pions, and of deuterons and charged kaons, in the interactions with a 5% λ_{abs} Be target of +8.9 GeV/*c* protons and pions, and of −8.0 GeV/*c* pions.

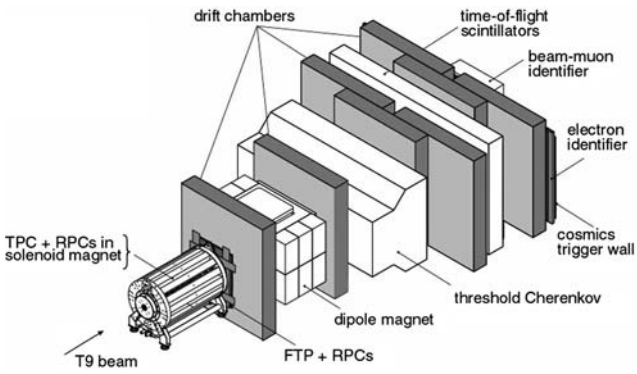

Fig. 1 Schematic view of the HARP detector

[a] e-mail: joerg.wotschack@cern.ch
[b] On leave of absence at Ecole Polytechnique Fédérale, Lausanne, Switzerland.

The data analysis presented in this paper rests exclusively on the calibrations of the TPC and the RPCs that we, the HARP–CDP group, published in [1] and [2]. As discussed in [3] and [4], and succinctly summarized in this paper's Appendix, our calibrations disagree with calibrations published by the 'HARP Collaboration' [5–8]. Conclusions of independent review bodies on the discrepancies between our results and those from the HARP Collaboration can be found in [9, 10].

2 The T9 proton and pion beams

The protons and pions were delivered by the T9 beam line in the East Hall of CERN's Proton Synchrotron. This beam line supports beam momenta between 1.5 GeV/c and 15 GeV/c, with a momentum bite $\Delta p/p \sim 1\%$.

Beam particle identification was provided for by two threshold Cherenkov counters filled with nitrogen, and by time of flight over a flight path of 24.3 m. In the +8.9 GeV/c and −8.0 GeV/c beams, the pressure of the nitrogen gas was set such that protons were below threshold for Cherenkov light but pions above. The time of flight of each beam particle was measured by three scintillation counters with a precision of 106 ps.[1]

Figure 2(a) shows the relative velocity β from the beam time of flight of positive particles in the +8.9 GeV/c beam, with protons distinguished from 'pions'[2] by the absence of a beam Cherenkov signal. Vice versa, Fig. 2(b) shows the signal charge in one beam Cherenkov counter, with protons and pions distinguished by the signal charge in the other beam Cherenkov counter. All measurements are independent of each other and together permit a clean separation between protons and pions, respectively, with a negligible contamination of less than 0.1% by the other particle.

The pion beam had a contamination by muons from pion decays. This contamination was measured to be $(1.7 \pm 0.5)\%$ of the pion component of the +8.9 GeV/c beam [11]. For the −8.0 GeV/c beam, this contamination is $(1.9 \pm 0.5)\%$. The pion beam also had a contamination by electrons from converted photons from π^0 decays. This contamination was determined to be $(1.2 \pm 0.5)\%$ of the pion component of the +8.9 GeV/c beam [12]. We take the same electron fraction for the −8.0 GeV/c beam. For the determination of interaction cross-sections of pions, the muon and electron contaminations must be subtracted from the incoming flux of pion-like particles.

[1] Under stable conditions of the beam optics, such that an average particle velocity could be used, the time-of-flight precision could be improved to 77 ps; in our analysis, no use was made of this option.

[2] The 'pions' comprise small contaminations by muons and electrons, indistinguishable both by time of flight and by beam Cherenkov signals.

The beam trajectory was determined by a set of three multiwire proportional chambers (MWPCs), located upstream of the target, several metres apart. The transverse error of the projected impact point on the target was 0.5 mm from the resolution of the MWPCs, plus a contribution from multiple scattering of the beam particles in various materials. Excluding the target itself, the latter contribution is 0.2 mm for a 8.9 GeV/c beam particle.

The size of the beam spot at the position of the target was several millimetres in diameter, determined by the setting

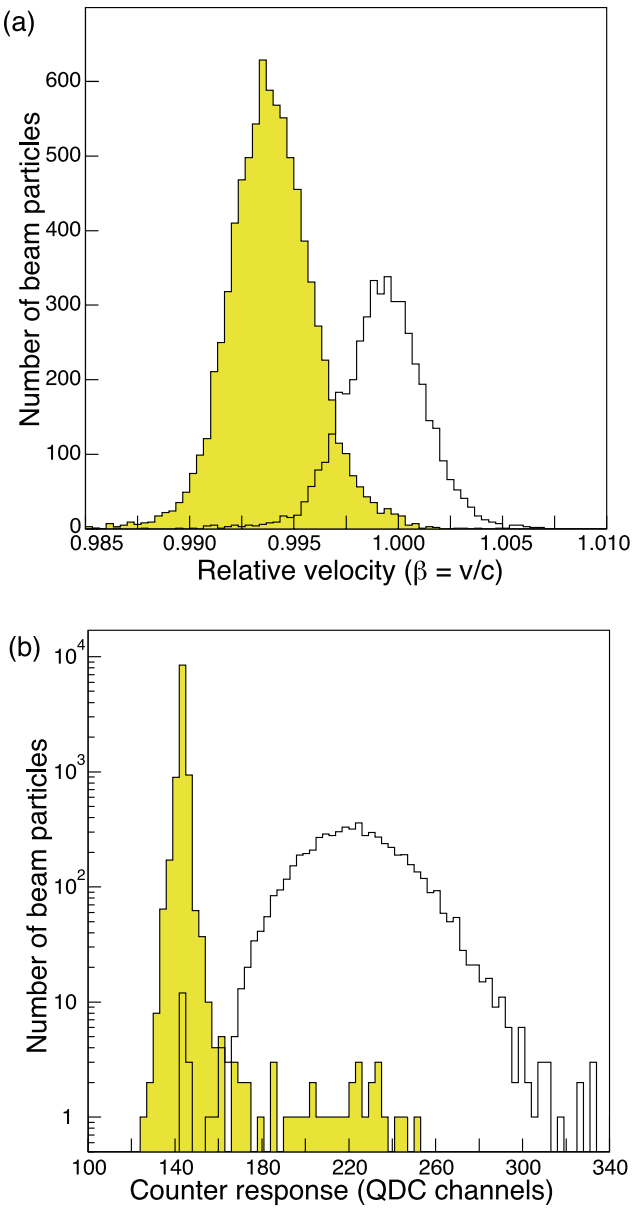

Fig. 2 (**a**) Relative velocity β from the beam time-of-flight system of protons (*shaded histogram*) and pions, with the particles identified in the beam Cherenkov counters; (**b**) charge response of the light signal in one beam Cherenkov counter from protons (*shaded histogram*) and pions, with the particles identified in the other beam Cherenkov counter

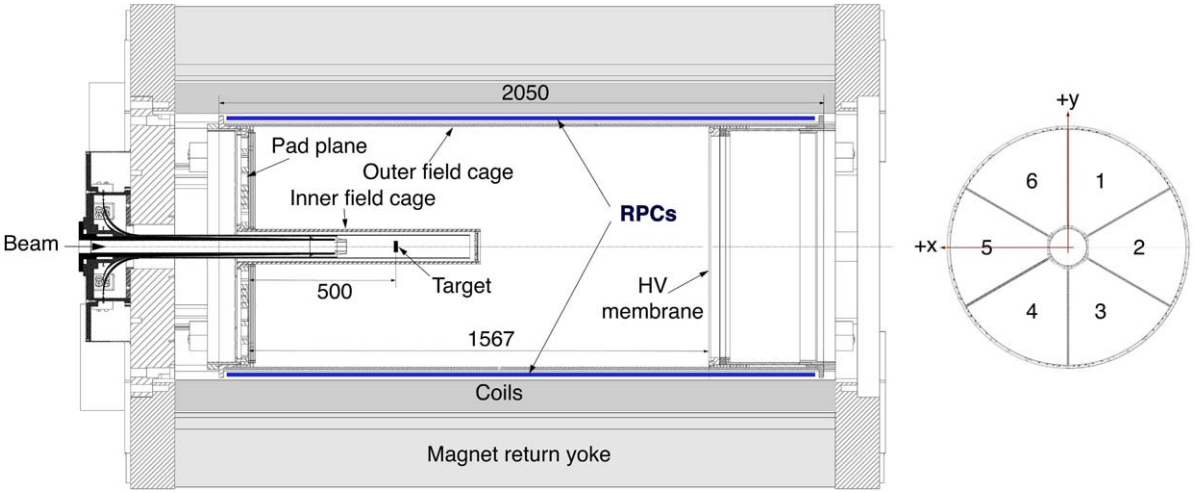

Fig. 3 Longitudinal cut through the TPC and the solenoidal magnet; the beam enters from the *left side*; the small figure to the *right* shows the layout of the six TPC readout sectors, looking downstream

of the beam optics and by multiple scattering. The nominal beam position[3] was at $x_{\text{beam}} = y_{\text{beam}} = 0$, however, excursions by several millimetres could occur.[4] A loose fiducial cut $\sqrt{x^2_{\text{beam}} + y^2_{\text{beam}}} < 12$ mm ensured full beam acceptance. The muon and electron contaminations of the pion beam, stated above, refer to this acceptance cut.

We select 'good' beam particles by requiring the unambiguous reconstruction of the particle trajectory with good χ^2. In addition we require that the particle type is unambiguously identified. We select 'good' accelerator spills by requiring minimal intensity and a 'smooth' variation of beam intensity across the 400 ms long spill.[5]

3 The large-angle spectrometer

In HARP's large-angle region, a cylindrical TPC [1] had been chosen as tracking detector. It was embedded in a solenoidal magnet that generated a magnetic field of 0.7 T parallel to the TPC axis. The magnet was in general operated with its polarity tied to the beam polarity.[6]

The TPC filled most of the inner bore of the magnet, leaving a 25 mm wide gap between TPC and magnet coils. This gap was used to house two overlapping layers of 2 m long RPCs [2] directly mounted onto the outer field cage of the TPC.

The layout of the TPC and its position in the solenoidal magnet is shown in Fig. 3. The TPC has an external diameter of 832 mm and an overall length of ∼2 m. It consists of two Stesalit cylinders forming the inner and outer field cages, a wire chamber with pad readout, located at the upstream end, and a high-voltage (HV) membrane at 1567 mm distance from the pad plane. The inner field cage extends over about half of the drift volume; it encloses the target, the centre of which is located 500 mm downstream of the pad plane.

The tracking volume extends radially from 75 mm to 385 mm and over ∼1.5 m longitudinally. Electrons from ionization induced by charged particles in the TPC gas drift upstream under the influence of the longitudinal electrical field; they are amplified in the wire chamber and read out through pads arranged in six identical sectors, as shown in Fig. 3. Each sector comprised 662 readout pads of dimensions 6.5×15 mm^2 arranged in 20 concentrical rows.

Our calibration work on the HARP TPC and RPCs is described in [1] and [2], and in references cited therein. In particular, we recall that static and dynamic TPC track distortions up to ∼10 mm have been corrected to better than 300 μm. Therefore, TPC track distortions do not affect the precision of our cross-section measurements.

[3] A right-handed Cartesian and/or spherical polar coordinate system is employed; the z axis coincides with the beam line, with $+z$ pointing downstream; the coordinate origin is at the centre of the beryllium target, 500 mm downstream of the TPC's pad plane; looking downstream, the $+x$ coordinate points to the left and the $+y$ coordinate points up; the polar angle θ is the angle with respect to the $+z$ axis; when looking downstream, the azimuthal angle ϕ increases in the clockwise direction, with the $+x$ axis at $\phi = 0$.

[4] The only relevant issue is that the trajectory of each individual beam particle is known, whether shifted or not, and therefore the amount of matter to be traversed by the secondary hadrons.

[5] A smooth variation of beam intensity eases corrections for dynamic TPC track distortions.

[6] The HARP data-taking convention was that $B_z > 0$ refers to positive beam polarity.

4 Track reconstruction and particle identification

4.1 Pattern recognition in the TPC

The clusters measured by the TPC constitute space points along the track trajectory. Each space point has three uniquely determined coordinates: r, ϕ, and z. Our pattern recognition of tracks with $p_{\mathrm{T}} \geq 0.05$ GeV/c originating from the target region is based on the TOPAZ histogram technique [13]: a 2-dimensional histogram of the ratio z/r against azimuthal angle ϕ is filled with all reconstructed clusters. Physical tracks populate one or two adjacent bins (the bin sizes are suitably chosen) and thus are easily recognised.

4.2 Helix fit of TPC tracks

For the fit of trajectories in the TPC we adopted the 'Generalized Least-Squares Fit' (GLSF) concept. This is the formal generalization of the standard least-squares fit for an arbitrary number of error-prone dimensions, and the solution of the equations resulting from the χ^2 minimization with the Lagrange-multiplier method. The mathematical intricacies can be found in [14]. For the three parameters that describe the circle projection of a helix, we adopted the TOPAZ parametrization [15], for the attractive feature of avoiding any discontinuity in the numerical values of fit parameters. Most importantly, it features a smooth transition between the left and the right bend of high-p_{T} tracks in the solenoidal magnetic field, and hence avoids a discontinuity in the assignment of a positive or negative charge-signed p_{T}. For more details on the parametrization and the fit procedure, we refer to [16].

The GLSF must start from reasonable starting values of the parameters that describe the helix. They are obtained by the Chernov–Ososkov algorithm [17].

Our GLSF algorithm yields the transverse momentum p_{T} of a track, its charge sign, its polar angle θ, and its closest point of approach to the z axis.

4.3 Virtual beam point

The p_{T} resolution of tracks can be improved by nearly a factor of two by the use of the beam point[7] as an additional point to the trajectory in the TPC. The transverse coordinates of the beam point are known from the extrapolation of the trajectory of the incoming beam particle. Their errors stem from the extrapolation of the beam trajectory that is measured by MWPCs, and from multiple scattering of the beam particle. When the beam point is used in the fit, a third contribution to the error of its transverse coordinates arises from multiple scattering of the secondary particle in materials between the vertex and the TPC volume.

However, the correct error assignment to the beam point is not sufficient. Since a secondary track loses energy by ionization in the target and in materials between the vertex and the TPC volume, a correction must be calculated that replaces the real beam point by a 'virtual' beam point which is bias-free with respect to the extrapolation of the trajectory measured in the TPC. It is this virtual beam point, and not the real beam point, that is used in the (final) track fit. It is determined in an iterative procedure that starts from the fit of the track momentum in the TPC gas, including the real beam point. The fitted trajectory in the TPC gas is then backtracked to the beam particle trajectory taking the energy loss and multiple scattering into account. It renders a first estimate of the virtual beam point. Using this estimate, the track in the TPC gas is again fitted, and the procedure is iterated until the position of the virtual beam point is stable. Since in the calculation of the move from the real to the virtual beam point the energy loss is taken into account, and since the energy loss depends on the type of particle, three different virtual beam points are calculated according to the proton, pion, and electron hypotheses. Accordingly, three different track fits are performed.

The fit with the virtual beam point included gives the best possible estimate of the particle momentum in the TPC gas. In order to determine what is really needed, namely the momentum at the vertex, in a last step the particle is tracked back to the vertex, taking into account the energy loss under the three different particle hypotheses. The track parameters at the vertex are used for the determination of differential cross-sections.

4.4 Particle identification algorithm

The particles detected in HARP's large-angle region are protons, charged pions, and electrons[8] (we disregard here small admixtures of kaons and deuterons which will be discussed in Sect. 7). The charged pion sample comprises muons from pion decay since the available instrumentation does not distinguish them from charged pions.

The $\mathrm{d}E/\mathrm{d}x$ and the time-of-flight methods of particle identification are considered independent.

To separate measured particles into species, we assign to each particle a probability of being a proton, a pion (muon), or an electron, respectively. The probabilities add up to unity, so that the number of particles is conserved.

Each track is characterized by four measured quantities: p_{T} (transverse momentum), θ (polar angle), β (relative velocity) and $\mathrm{d}E/\mathrm{d}x$ (specific ionization). For particle identification purposes, these variables refer to reconstructed

[7] What we call 'beam point' is the best estimate of the interaction vertex of the incoming beam particle.

[8] The term 'electron' also refers to positrons.

('smeared') variables in both the data and the Monte Carlo simulation.

In every bin of (p_T, θ), the probability $\mathcal{P}(i|\beta, dE/dx, p_T, \theta)$ of a particle to belong to species i ($i = 1$ [proton], 2 [pion], 3 [electron]) in a mixture of protons, pions, and electrons is according to Bayes' theorem as follows:

$$\mathcal{P}(i|\beta, dE/dx, p_T, \theta) = \frac{P(\beta, dE/dx|i, p_T, \theta) \cdot P(i, p_T, \theta)}{\sum_{i=1}^{3}[P(\beta, dE/dx|i, p_T, \theta) \cdot P(i, p_T, \theta)]}, \quad (1)$$

where the sum

$$\sum_{i=1}^{3} \mathcal{P}(i|\beta, dE/dx, p_T, \theta)$$

is normalized to unity. The probabilities $P(i, p_T, \theta)$ are given by

$$P(i, p_T, \theta) = \frac{N_i(p_T, \theta)}{\sum_{i=1}^{3} N_i(p_T, \theta)},$$

where $N_i(p_T, \theta)$ is the number of particles of species i in the respective data sample. Then (1) becomes

$$\mathcal{P}(i|\beta, dE/dx, p_T, \theta) = \frac{P(\beta, dE/dx|i, p_T, \theta) \cdot N_i(p_T, \theta)}{\sum_{i}^{3}[P(\beta, dE/dx|i, p_T, \theta) \cdot N_i(p_T, \theta)]}. \quad (2)$$

We note that in (1) and (2) the term $P(\beta, dE/dx|i, p_T, \theta)$ denotes a probability density function which is normalized to unity. This probability density function must represent the data in the bin (p_T, θ).

Before determining the probability represented by (2), the probability density functions $P(\beta, dE/dx|i, p_T, \theta)$ and the particle abundances $N_i(p_T, \theta)$ must be known. This seemingly circular situation is resolved by an iterative comparison of data with the Monte Carlo simulation, to achieve agreement of the distributions in both variables β and dE/dx. With a view to starting from abundances as realistic as possible, the comparison is initially limited to regions in phase space where the particle species are unambiguously separated from each other in either dE/dx or β. In other words, the few parameters that govern the probability density functions and the particle abundances are determined from the data in every bin of (p_T, θ).

In case one of the two identification variables is absent,[9] only the other is used. In the rare cases where both identification variables are absent, the identification probabilities reproduce the estimated particle abundances.

[9]For example, because of too few clusters to calculate dE/dx, or a missing RPC pad.

4.5 Particle abundances

Particle abundances cannot *a priori* be expected to be correct in the Monte Carlo simulation. Therefore in general the particles must be weighted such that data and Monte Carlo distributions agree.

We had expected that the Monte Carlo simulation tool kit Geant4 [18, 19] would provide us with reasonably realistic spectra of secondary hadrons. We found this expectation more or less met by Geant4's so-called QGSP_BIC physics list, but only for the secondaries from incoming beam protons. For the secondaries from incoming beam pions, we found the standard physics lists of Geant4 unsuitable [20].

To overcome this problem, we built our own HARP_CDP physics list for the production of secondaries from incoming beam pions. It starts from Geant4's standard QBBC physics list, but the Quark–Gluon String Model is replaced by the FRITIOF string fragmentation model for kinetic energy $E > 6$ GeV; for $E < 6$ GeV, the Bertini Cascade is used for pions, and the Binary Cascade for protons; elastic and quasi-elastic scattering is disabled. Examples of the good performance of the HARP_CDP physics list are given in [20].

Figure 4 demonstrates the level of overall agreement between data and Monte Carlo simulation in the variable $1/p_T$, after convergence of the iterative procedure to determine the smooth weighting functions to the latter. The figure also shows, for incoming protons and for a typical polar-angle range, the subdivision of the data into particle species by applying the particle identification weights.

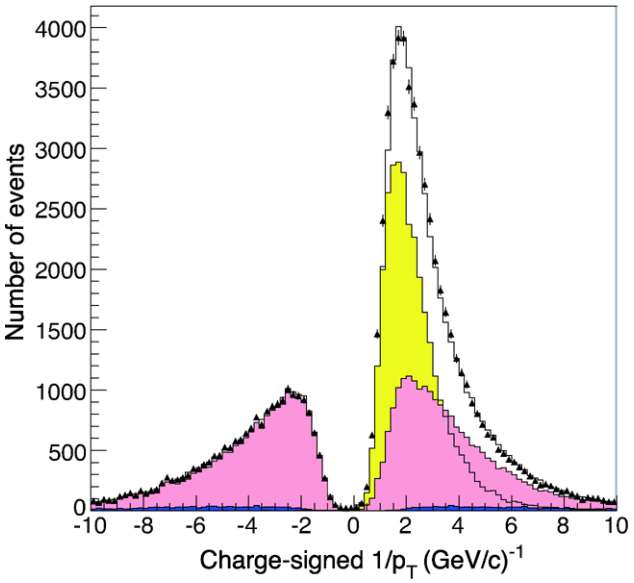

Fig. 4 $1/p_T$ spectra of the secondary particles from +8.9 GeV/c beam protons on a 5% λ_{abs} Be target, for polar angles $50° < \theta < 60°$; *black triangles* denote data, the *solid lines* Monte Carlo simulation; the *shaded histograms* show the subdivision of the data into particle species by applying the particle identification weights: *light shading* denotes protons, *medium shading* pions, and *dark shading* electrons

Once the abundances are determined, for any pair of dE/dx and β, and using the experimental resolution functions, the probability can be derived that the particle is a proton, a pion, or an electron. This probability is consistently used for weighting when entering tracks into plots or tables.

5 Physics performance

5.1 Physics performance of the TPC

In [1] the absolute momentum scale has been shown to be correct to better than 2%, both for positively and negatively charged particles.

Figure 5(a) shows the $1/p_T$ difference for positive particles with $0.6 < \beta < 0.75$ and $45° < \theta < 65°$, between the measurement in the TPC and the determination from RPC time of flight with the proton-mass hypothesis. The selection cuts ensure a practically pure sample of protons (the background from pions and kaons is negligible as suggested by the very small contribution of negative particles selected with the same cuts that are shown as dots in Fig. 5(a)). A net TPC resolution of $\sigma(1/p_T) = 0.20$ $(\text{GeV}/c)^{-1}$ is obtained by subtracting the contribution of ~ 0.18 $(\text{GeV}/c)^{-1}$ from the time-of-flight resolution and fluctuations from energy loss and multiple scattering in materials between the vertex and the TPC volume quadratically from the convoluted resolution of 0.27 $(\text{GeV}/c)^{-1}$.

Figure 5(b) shows the net TPC resolution $\sigma(1/p_T)$ as a function of β. Figure 5(c) shows the same as a function of θ. The agreement with the expectation from a Monte Carlo simulation is satisfactory. The resolution $\sigma(1/p_T)$ is typically 0.2 $(\text{GeV}/c)^{-1}$ and worsens towards small β and small θ. This is because in both cases the position error of the virtual beam point increases owing to increased multiple scattering in materials before the protons enter the TPC.

Data from the elastic scattering of incoming pions or protons on protons at rest have the added feature of a kinematical constraint. The possibility to calculate from the four-momentum of the incoming beam particle and the polar angle θ the momentum of the large-angle recoil proton, permits a valuable cross-check of the TPC's p_T resolution. Figure 6 shows the result from the elastic scattering of incoming $+3$ GeV/c protons and π^+'s in a liquid hydrogen target. Here, the p_T of the recoil proton has been determined in the following two ways: $1/p_T^{\text{meas}}$ is determined from the reconstructed track curvature in the TPC; $1/p_T^{\text{pred}}$ is predicted from the elastic scattering kinematics from the polar angle of the recoil proton which is little affected by TPC track distortions. Figure 6 demonstrates a resolution of $\sigma(1/p_T) \sim 0.19$ $(\text{GeV}/c)^{-1}$ after unfolding a contribution of $\sigma(1/p_T) \sim 0.12$ $(\text{GeV}/c)^{-1}$ from fluctuations from energy loss and multiple scattering in materials between the vertex and the TPC volume. The measured difference in p_T is 0.8%, in line with the 2% uncertainty of the momentum scale.

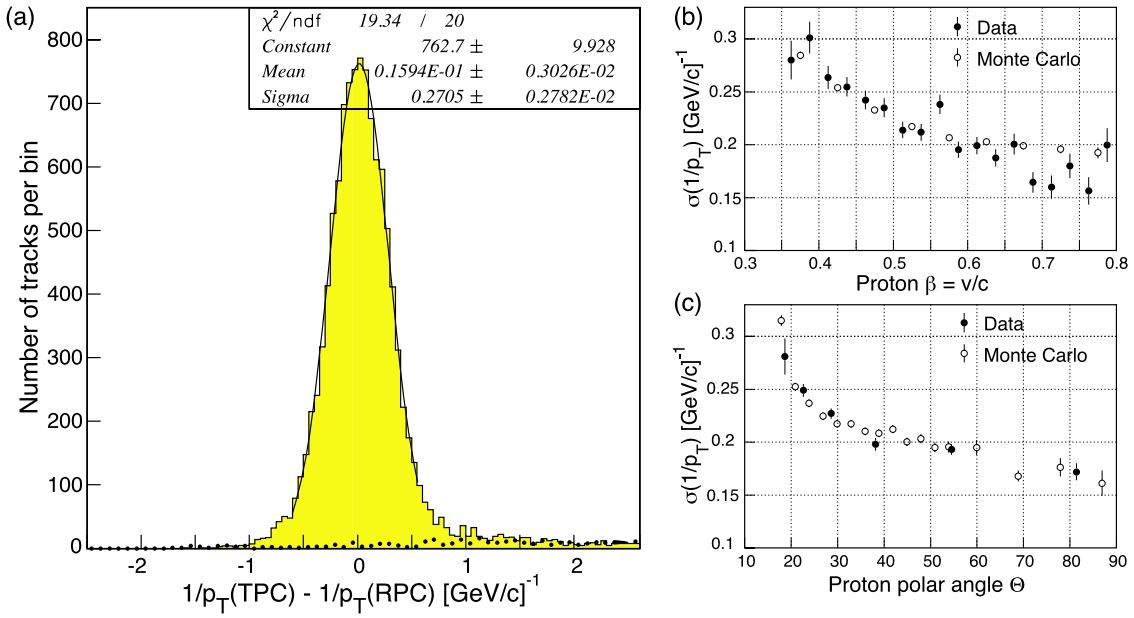

Fig. 5 (**a**) Difference of the inverse transverse momenta of positive (*shaded histogram*) and negative (*dots*) particles from the measurement in the TPC and from the determination from RPC time of flight, for $0.6 < \beta < 0.75$ and for $45° < \theta < 65°$; the positive particles are protons, with a very small background from pions and kaons; (**b**) $\sigma(1/p_T)$ of protons with $45° < \theta < 65°$ as a function of their relative velocity β; (**c**) $\sigma(1/p_T)$ of protons with $0.6 < \beta < 0.75$ as a function of their polar angle θ

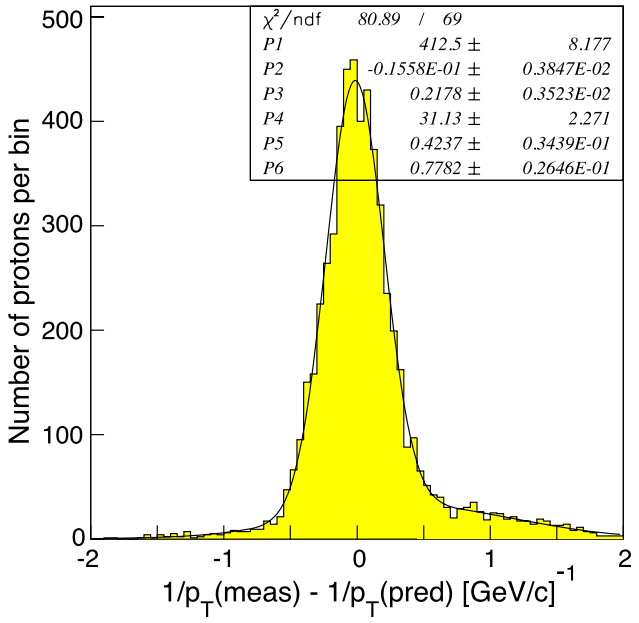

Fig. 6 The difference $1/p_{\mathrm{T}}^{\mathrm{meas}} - 1/p_{\mathrm{T}}^{\mathrm{pred}}$ from large-angle recoil protons in elastic scattering events from a +3 GeV/c beam impinging on a liquid hydrogen target; the tail at the *right side* reflects the Landau tail in the proton energy loss in materials between the interaction point and the TPC volume

The polar angle θ is measured in the TPC with a resolution of ∼9 mrad, for a representative angle of $\theta = 60°$. To this a multiple scattering error has to be added which is ∼7 mrad for a proton with $p_{\mathrm{T}} = 500$ MeV/c and $\theta = 60°$, and ∼4 mrad for a pion with the same characteristics. The polar-angle scale is correct to better than 2 mrad.

Besides the p_{T} and the polar angle θ of tracks, the TPC also measures $\mathrm{d}E/\mathrm{d}x$ with a view to particle identification. The $\mathrm{d}E/\mathrm{d}x$ resolution is 16% for a track length of 300 mm.

5.2 Physics performance of the RPCs

The intrinsic efficiency of the RPCs that surround the TPC is better than 98%. While the system efficiency for pions with $p_{\mathrm{T}} > 100$ MeV/c at the vertex is close to the intrinsic efficiency, it is slightly worse for protons because of their higher energy loss in structural materials. Protons with $p <$ 350 MeV/c at the vertex get absorbed before they reach the RPCs and thus escape time-of-flight measurement.

The intrinsic time resolution of the RPCs is 127 ps and the system time-of-flight resolution (that includes the jitter of the arrival time of the beam particle at the target) is 175 ps.

Figure 7(a) shows the specific ionization $\mathrm{d}E/\mathrm{d}x$, measured by the TPC, and Fig. 7(b) the relative velocity β from the RPC time of flight, of positive and negative secondaries, as a function of the momentum measured in the TPC. The figures demonstrate that in general protons and pions are well separated. They also underline the importance of the complementary separation by RPC time of flight at large particle momentum.

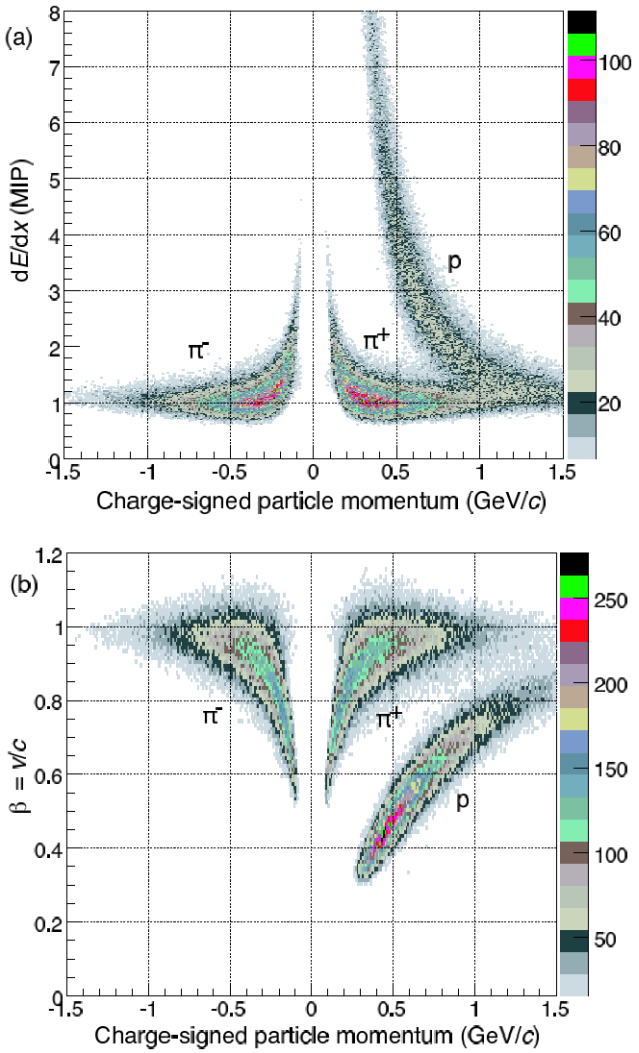

Fig. 7 (**a**) Specific ionization $\mathrm{d}E/\mathrm{d}x$ and (**b**) velocity β, versus the charge-signed momentum of positive and negative tracks in +8.9 GeV/c data; the *boxes at the right side* indicate the event statistics

6 Normalized secondary particle flux

The measurement of the inclusive double-differential cross-section $\mathrm{d}^2\sigma/\mathrm{d}p\mathrm{d}\Omega$ requires the flux of incoming beam particles, the number of target nuclei, and the number of secondary particles in bins of momentum p and polar angle θ. We shall discuss these elements in turn.

6.1 Beam intensity

The event trigger had two levels. A first, loose, level required only time-coincident signals from beam scintillation coun-

ters. Irrespective of an interaction in the target, each 64th coincidence signal requested data readout as 'beam trigger'. A second, tighter level required in addition a signal in a cylindrical scintillator fibre detector that surrounded the target region, or a signal in a plane of scintillators in the forward direction (termed 'FTP' in Fig. 1). Each such 'event trigger' also requested data readout.

To achieve the wanted event statistics, the experiment was typically run with a dead time in excess of 50%, given the 400 ms long accelerator spill and a readout time of order 1 ms per event. Since the dead time affects the beam trigger and the event trigger in the same way, it cancels in the cross-section calculation. For a given data set, the flux of incoming beam particles is defined by the number of beam triggers, multiplied by the scale-down factor of 64. It is imperative, though, that the same cuts on the quality of the trajectory of the beam particle and on its identification be applied for accepted beam triggers and for accepted event triggers.

The efficiencies of both the beam trigger and the event trigger are very close to 100%, thanks to majority requirements. The beam trigger efficiency cancels. For the event trigger, we determined an efficiency of $(99.0 \pm 0.2)\%$.

6.2 Target

The target was a cylinder made of high-purity (99.95%) beryllium, with a density of 1.85 g/cm^3, a radius of 15 mm, and a thickness of 20.5 ± 0.1 mm (5% λ_{abs}).

The finite thickness of the target leads to a small attenuation of the number of incident beam particles. The attenuation factor is $f_{\mathrm{att}} = 0.975$.

6.3 Track counting in bins of p_{T} and θ

This paper is concerned with determining inclusive cross-sections of secondaries from the interactions of protons and pions with beryllium nuclei. This means that for a given data set, the secondaries are weighted with their probability of being a proton, a pion, or an electron, counted in bins of p_{T} and θ, and related to the number of incoming beam particles and the number of target nuclei. The counting of secondaries is done in an integral way without regard to track–event relations.

Electrons stem primarily from the conversion of photons from π^0 decays. They tend to concentrate at small momenta. Below 150 MeV/c, they are identified by both $\mathrm{d}E/\mathrm{d}x$ and time of flight from the RPCs. From 150 to 250 MeV/c, the $\mathrm{d}E/\mathrm{d}x$ of pions and electrons coincides and they are only identified by time of flight. The Geant4 electron abundance is compared with data in the region of good separation, as a function of momentum, and weighted to agree with the data. In the region of bad separation the electrons are subtracted using not the electron abundance predicted by Geant4, but the weighted prediction extrapolated from the region of good separation. Therefore, the Geant4 prediction is used only through its extrapolated prediction of the energy dependence of electrons with momentum larger than 250 MeV/c.

Since the particle identification algorithm assigns to every particle a probability of being a proton, a pion, or an electron, the elimination of electrons from the samples of secondary protons and pions is straightforward.

It is justified to think of secondary tracks as originating exclusively from proton and pion interactions: interactions of beam electrons might occasionally lead to low-momentum electron or positron tracks in the TPC, however, such tracks are recognized by the particle identification algorithm and disregarded in hadron production cross-sections. Interactions of beam muons can be neglected.

Kaon and deuteron secondaries are initially part of pions and protons, respectively. Their identification is dealt with in Sect. 7.

6.4 Track selection cuts

We have a selection of 'good' TPC sectors: we discard tracks from the 'horizontal' sectors 2 and 5 out of the six sectors (see Fig. 3) for reasons of much worse than average performance, and the lack of reliable track distortion corrections [1].

Tracks are accepted if there are at least 10 TPC clusters along the trajectory.

A cut in the azimuthal angle ϕ is applied to avoid the dead regions of the six 'spokes' that subdivide the TPC pad plane into six sectors: 10° on one side and 2° on the other side of each spoke for tracks of one charge, and *vice versa* for the other charge. The asymmetric cut is motivated by the opposite bending of positive and negative tracks in the magnetic field.

The polar-angle range of tracks is limited to the range $20° < \theta < 125°$. Tracks are also required to point back to the target, within the resolution limits.

6.5 Correction for inefficiencies of track reconstruction and track selection

The track reconstruction efficiency was determined by eyeball scanning of several thousand events by several physicists, with consistent results among them. The large number of scanned events permits us to determine the reconstruction efficiency as a function of geometric or kinematic variables. For example, Fig. 8(a) shows the reconstruction efficiency as a function of $1/p_{\mathrm{T}}$ for all cases where the human eye finds at least five (out of a maximum of 20) clusters along a trajectory. The average reconstruction efficiency is between

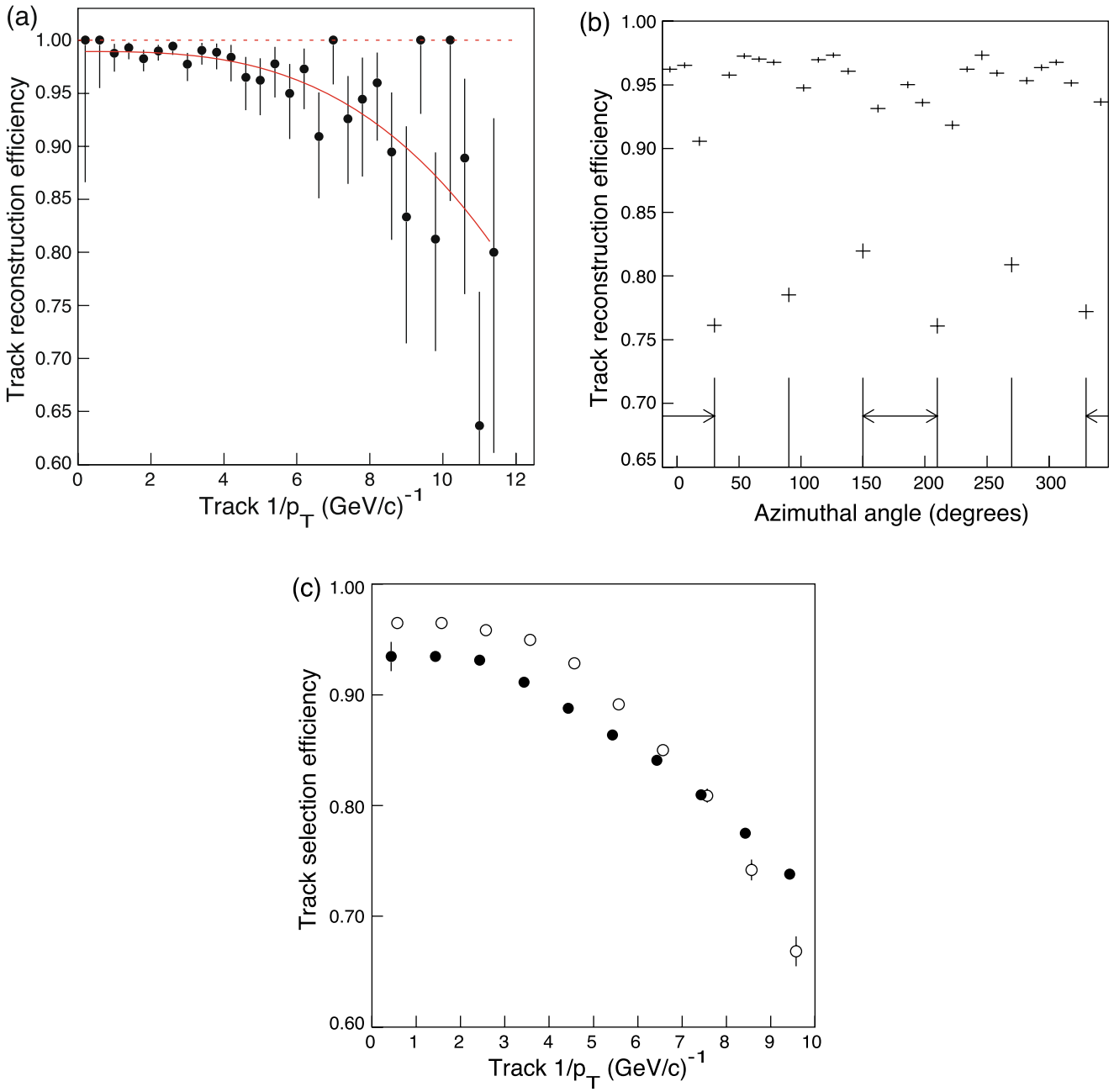

Fig. 8 (**a**) Track reconstruction efficiency from the eyeball scan; (**b**) track reconstruction efficiency from RPC hits; the vertical lines denote TPC sector boundaries where the TPC 'spokes' render the efficiency lower; the azimuthal ranges of the two TPC sectors not used for the analysis are indicated by arrows; (**c**) efficiency of 10 or more TPC clusters for protons (*open circles*) and for pions (*black circles*); the errors shown are statistical only and mostly smaller than the symbol size

95% and 97%,[10] where the 2% range reflects the variation between different data sets.

We cross-checked the track reconstruction efficiency by requiring an RPC hit and at least two TPC clusters in the cone that is subtended by the respective RPC pad, as seen from the vertex. Figure 8(b) shows the resulting reconstruction efficiency as a function of the track's azimuthal angle. Outside the TPC spokes and within the four 'good' TPC sectors, the reconstruction efficiency determined that way agrees with the result from the eyeball scan.

The requirement of a minimum of 10 TPC clusters per track entails a loss that must be accounted for. Since the

[10]This average holds for tracks with $|p_T| > 0.1$ GeV/c and $20° < \theta < 125°$, with safe distance from the insensitive azimuthal regions caused by the TPC 'spokes'.

TPC cluster charge is in general larger for protons[11] than for pions, the loss from this cut is different for protons and pions. Figure 8(c) shows the efficiency of requiring 10 or more TPC clusters, determined from the data, as a function of $1/p_{\mathrm{T}}$, separately for protons and pions (the average number of clusters was $\sim$14).

The overall track efficiency was taken as the product of the track reconstruction efficiency and the probability of having at least 10 clusters along the trajectory.

6.6 Further corrections

In this section, we discuss a few more corrections that are applied to the data. In general, they are determined from a Monte Carlo simulation that reproduces the migration of track parameters from generated ('true') to reconstructed ('smeared') ones. This concerns effects arising from finite resolution, charge misidentification, pion decays into muons, and re-interactions of secondaries in materials between the vertex and the TPC volume.[12] There is also backscattering of particles from the solenoid coil at large radius back into the TPC, however, tracks from backscattering are eliminated by the requirement that they originate from the target.

Other than for the transverse momentum p_{T}, migration is nearly negligible in the measurement of the polar angle θ.

Charge misidentification occurs only at large transverse momentum, at the level of a few per cent. For example, a few 'antiprotons' at large transverse momentum are charge-misidentified protons and treated accordingly in the migration correction.

Pion decay into muons occurs at the typical level of 2%. When the pion decay occurs in the first few centimetres of the flight path, the phenomenon is taken care of by the migration correction. When the pion decay occurs later, the track is likely to be lost because of the requirement that it originates from the target. Therefore, each pion receives a weight that compensates on the average for the loss from decay along a path of 200 mm length.

The re-interaction of secondaries takes place in the target material or in other materials between the target and the TPC volume. The typical probability for re-interaction is 3% for the former, and 2% for the latter. The re-interaction leads to tracks with other parameters than the initial track, and is taken care of by the migration correction.

[11] The lower proton velocity leads to higher specific ionization.

[12] These re-interactions, especially in the target material, are different from re-interactions of secondaries in the nuclear matter of the same nucleus in which the incoming beam particle interacted; the latter is an integral part of the inclusive cross-section reported in this paper.

6.7 Systematic errors

The systematic precision of our inclusive cross-sections is at the few-per-cent level, from errors in the normalization, in the momentum measurement, in particle identification, and in the corrections applied to the data.

The systematic error of the absolute flux normalization is taken as 2%. This error arises from uncertainties in the target thickness, in the contribution of large-angle scattering of beam particles, in the attenuation of beam particles in the target, and in the subtraction of the muon and electron contaminations. Another contribution comes from the removal of events with an abnormally large number of TPC hits above threshold.[13]

The systematic error of the track finding efficiency is taken as 1% which reflects differences between results from different persons who conducted eyeball scans. We also take the statistical errors of the parameters of a fit to scan results as shown in Fig. 8(a) as systematic error into account. The systematic error of the correction for losses from the requirement of at least 10 TPC clusters per track is taken as 20% of the correction which itself is in the range of 5 to 30%. This estimate arose from differences between the four TPC sectors that were used in our analysis, and from the observed variations with time.

The systematic error of the p_{T} scale is taken as 2% as discussed in [1].

The systematic errors of the proton, pion, and electron abundances are taken as 10%. We stress that errors on abundances only lead to cross-section errors in case of a strong overlap of the resolution functions of both identification variables, $\mathrm{d}E/\mathrm{d}x$ and β. The systematic error of the correction for migration, absorption of secondary protons and pions in materials, and for pion decay into muons, is taken as 20% of the correction, or 1% of the cross-section, whichever is larger. These estimates reflect our experience with remanent differences between data and Monte Carlo simulations after weighting Monte Carlo events with smooth functions with a view to reproducing the data simultaneously in several variables in the best possible way.

All systematic errors are propagated into the momentum spectra of secondaries and then added in quadrature.

7 Kaon and deuteron production

The statistics from the +8.9 GeV/c beam on a 5% λ_{abs} beryllium target is much larger than for any other combination of beam and target. This permits us to investigate in

[13] Very rarely, because of apparatus malfunction, the number of TPC hits was much larger than possible for a physics event. Such events are considered unphysical and eliminated.

this particular data set the production of K^+'s and deuterons in addition to the dominant protons, π^+'s, and π^-'s. With a view to benefiting from the cancellation of systematic errors, we present results in terms of the ratios K^+/π^+ and d/p.

7.1 Kaons

Figure 9 shows the relative velocity β of positive secondaries for the polar-angle range $20.5° < \theta < 25.3°$ and momentum between 520 and 560 MeV/c. A logarithmic scale is employed to make K^+ production visible which is at the level of a few per cent of the π^+ production. The K^+ signal shows up between the proton and π^+ signal thanks to the good resolution of the β measurement by the RPCs.

The K^+ signal is fitted with a Gaussian. The π^+ signal is represented by a Gaussian together with a tail that is experimentally determined from the β distribution of the π^-'s. The latter is shown with crosses in Fig. 9. A possible K^- contribution is minimized by a dE/dx cut.

In order to maximize the time of flight and hence the separation power, we restrict the analysis to the forward region in the range $20° < \theta < 32°$. The momentum is required to be in the range $400 < p < 700$ MeV/c, and dE/dx must be between 70% and 155% of the nominal value.

Several corrections must be made to the fit results of the relative K^+ abundance. Correcting for cuts on the charge of the RPC signal, made with a view to optimizing time-of-flight resolution, reduces the signal by 5%. The correction for the non-Gaussian tail of the β distribution of K^+'s increases the signal by 8%. The correction for different absorption of K^+'s and π^+'s in structural materials increases the signal by 1%.

Altogether, the resulting ratio is

$$R_K(p,\theta) = \frac{d^2\sigma_K(p,\theta)/dp d\Omega}{d^2\sigma_\pi(p,\theta)/dp d\Omega} = 0.020 \pm 0.003,$$

averaged over the said range of momentum and polar angle, and over the proton and π^+ beams (in kaon production, no significant difference is seen between these beams). Figure 10 shows the K^+/π^+ ratio as a function of particle momentum and compares the measured ratios with the ratios from the FRITIOF and Binary Cascade hadron production models in Geant4. The data points are closer to the prediction by the FRITIOF model, however, the dependence on momentum is not reproduced. The agreement with the Binary Cascade model is poor.

7.2 Deuterons

Figure 11 shows the dE/dx of positive secondaries for the polar-angle range $30° < \theta < 45°$ and the momentum range from 500 to 600 MeV/c (this momentum range refers to the momentum measured in the TPC and not to the momentum at the vertex). Pions and electrons are reduced by a loose time-of-flight cut. A clear signal of deuterons is visible at large dE/dx, next to the abundant protons.

In order to transform the ratio measured in the TPC volume to that at the vertex, appropriate corrections for the dif-

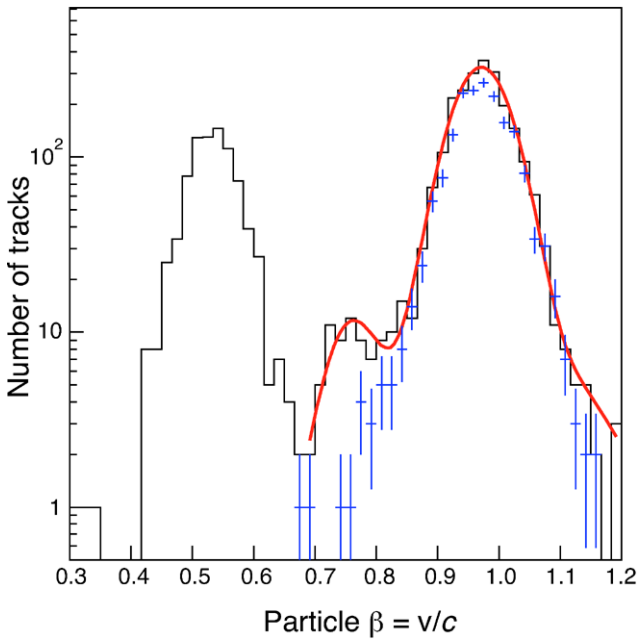

Fig. 9 Distribution of β of positive secondaries on a logarithmic scale, with the K^+ signal showing up between pions and protons; the crosses show the β distribution of π^-'s; the shown fit is explained in the text

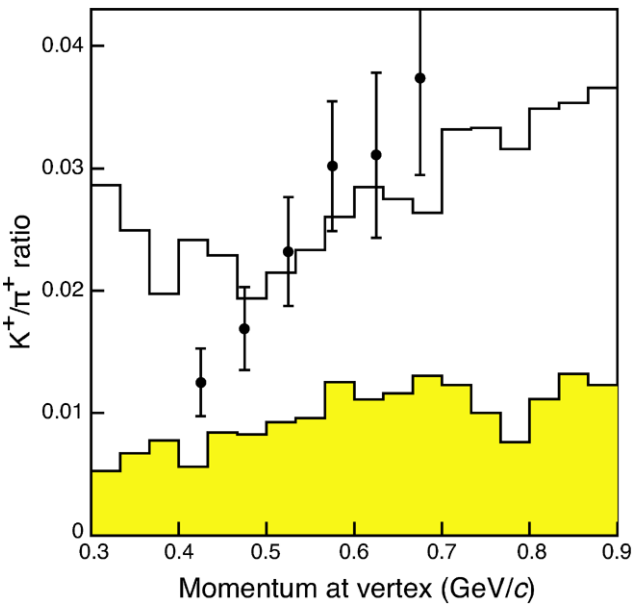

Fig. 10 Ratio of K^+/π^+ in +8.9 GeV/c proton and π^+ interactions with beryllium nuclei; the data points (*black circles*) are closer to the prediction by the FRITIOF model (*open histogram*) in Geant4, but agree poorly with its Binary Cascade model (*shaded histogram*)

Table 1 Ratio R_d of deuterons to protons, for different beam particles, averaged over the momentum at the vertex between 600 MeV/c and 1050 MeV/c

	+8.9 GeV/c protons	+8.9 GeV/c π^+	−8.0 GeV/c π^-
$20° < \theta < 30°$	0.051 ± 0.004	0.038 ± 0.004	0.05 ± 0.01
$30° < \theta < 45°$	0.076 ± 0.004	0.065 ± 0.005	0.07 ± 0.01
$45° < \theta < 65°$	0.113 ± 0.009	0.094 ± 0.008	0.13 ± 0.02
$65° < \theta < 90°$	0.17 ± 0.03	0.15 ± 0.03	0.16 ± 0.03
$90° < \theta < 125°$	0.26 ± 0.04	0.21 ± 0.05	0.30 ± 0.05

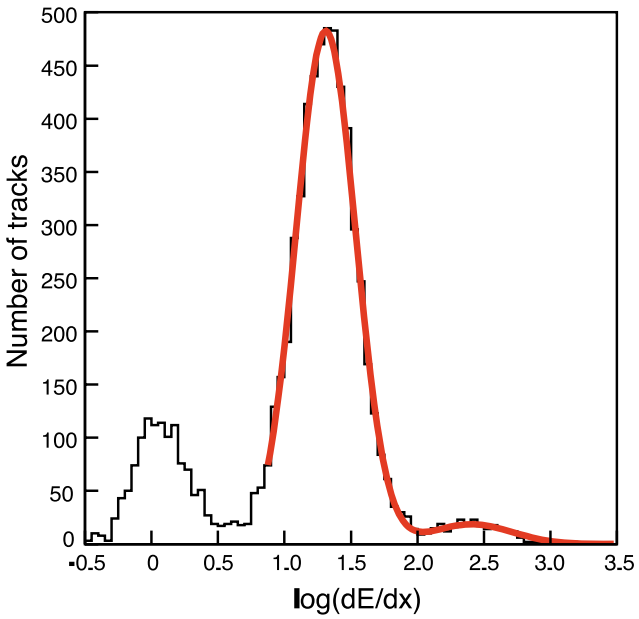

Fig. 11 Distribution of dE/dx of positive secondaries, with the deuteron signal showing up at large dE/dx; see the text for the cuts applied; both the proton and deuteron signals are fitted with a Gaussian

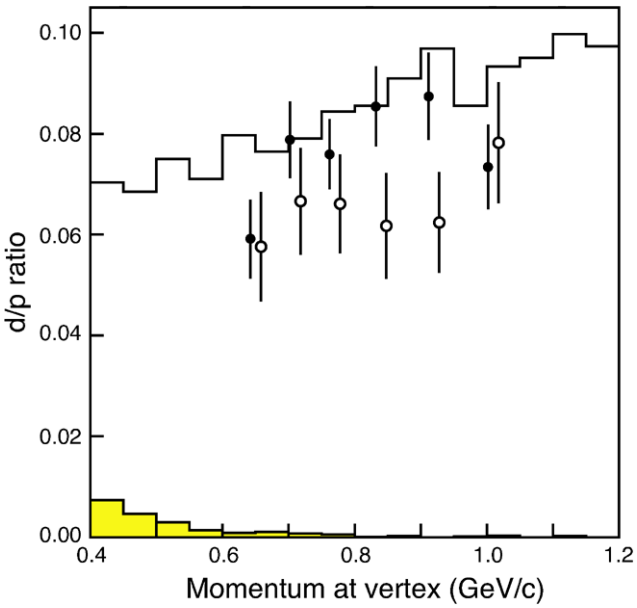

Fig. 12 Ratio R_d in +8.9 GeV/c proton and π^+ interactions with beryllium nuclei, for $30° < \theta < 45°$, as a function of the momentum at the vertex; *black data points* refer to the proton beam, *open circles* to the π^+ beam. The proton beam data are compared with the predictions of the FRITIOF (*open histogram*) and the Binary Cascade (*shaded histogram*) models in Geant4

ferent energy loss of protons and deuterons in materials between the vertex and the TPC volume, and for differences in the momentum spectra of protons and deuterons, must be applied. The results for the ratio

$$R_d(p,\theta) = \frac{d^2\sigma_d(p,\theta)/dp d\Omega}{d^2\sigma_p(p,\theta)/dp d\Omega},$$

averaged over the momentum at the vertex between 600 MeV/c and 1050 MeV/c, are given in Table 1.

The ratios R_d for the +8.9 GeV/c proton and π^+ beams are shown in Fig. 12 for the polar-angle range $30° < \theta < 45°$ as a function of the momentum at the vertex. We note that the deuteron abundance is reasonably well reproduced by the FRITIOF String Fragmentation model used in the Geant4 simulation tool kit, while it is underestimated by about one order of magnitude by the Binary Cascade model.

8 Double-differential inclusive cross-sections of protons and pions

In Tables 2–10 we give the double-differential inclusive cross-sections $d^2\sigma/dp d\Omega$ for all nine combinations of incoming beam particle and secondary particle, including statistical and systematic errors. In each bin, the average momentum and the average polar angle are also given.

Cross-sections are only given if the total error is not larger than the cross-section itself. Since our track reconstruction algorithm is optimized for tracks with p_T above ∼70 MeV/c in the TPC volume, we do not give cross-sections from tracks with p_T below this value. Because of the absorption of slow protons in the material between the vertex and the TPC gas, and with a view to keeping the correction for absorption losses below 30%, cross-sections from protons are limited to $p > 350$ MeV/c at the interaction vertex. Proton cross-sections are also not given if a 10%

Table 2 Double-differential inclusive cross-section $d^2\sigma/dpd\Omega$ [mb/(GeV/c sr)] of the production of protons in p + Be → p + X interactions with +8.9 GeV/c beam momentum; the first error is statistical, the second systematic; p_T in GeV/c, polar angle θ in degrees

p_T	$20 < \theta < 30$			$30 < \theta < 40$		
	$\langle p_T \rangle$	$\langle \theta \rangle$	$d^2\sigma/dpd\Omega$	$\langle p_T \rangle$	$\langle \theta \rangle$	$d^2\sigma/dpd\Omega$
0.20–0.24	0.220	24.9	$48.38 \pm 0.72 \pm 2.25$			
0.24–0.30	0.270	24.9	$48.68 \pm 0.59 \pm 2.02$	0.271	35.0	$42.76 \pm 0.54 \pm 1.65$
0.30–0.36	0.330	25.0	$44.77 \pm 0.55 \pm 1.66$	0.329	35.0	$41.00 \pm 0.52 \pm 1.39$
0.36–0.42	0.389	24.9	$41.06 \pm 0.53 \pm 1.41$	0.389	35.0	$38.10 \pm 0.51 \pm 1.20$
0.42–0.50	0.459	24.9	$39.55 \pm 0.45 \pm 1.26$	0.459	34.9	$33.39 \pm 0.42 \pm 1.00$
0.50–0.60	0.548	24.9	$34.14 \pm 0.37 \pm 1.11$	0.548	34.9	$27.89 \pm 0.34 \pm 0.87$
0.60–0.72	0.657	24.9	$27.82 \pm 0.31 \pm 1.05$	0.656	34.9	$21.47 \pm 0.27 \pm 0.80$
0.72–0.90				0.801	34.8	$14.52 \pm 0.19 \pm 0.74$
p_T	$40 < \theta < 50$			$50 < \theta < 60$		
	$\langle p_T \rangle$	$\langle \theta \rangle$	$d^2\sigma/dpd\Omega$	$\langle p_T \rangle$	$\langle \theta \rangle$	$d^2\sigma/dpd\Omega$
0.30–0.36	0.330	45.0	$38.81 \pm 0.50 \pm 1.15$			
0.36–0.42	0.389	45.0	$36.20 \pm 0.49 \pm 0.99$	0.390	55.0	$33.80 \pm 0.47 \pm 0.88$
0.42–0.50	0.458	44.9	$30.11 \pm 0.40 \pm 0.86$	0.458	54.9	$28.77 \pm 0.38 \pm 0.78$
0.50–0.60	0.548	44.9	$23.87 \pm 0.32 \pm 0.78$	0.548	55.0	$21.07 \pm 0.30 \pm 0.74$
0.60–0.72	0.656	44.9	$17.87 \pm 0.25 \pm 0.70$	0.655	54.9	$15.71 \pm 0.25 \pm 0.69$
0.72–0.90	0.801	44.8	$11.38 \pm 0.17 \pm 0.61$	0.798	54.8	$8.62 \pm 0.15 \pm 0.51$
0.90–1.25	1.035	44.7	$3.96 \pm 0.07 \pm 0.35$	1.033	54.7	$2.39 \pm 0.06 \pm 0.25$
p_T	$60 < \theta < 75$			$75 < \theta < 90$		
	$\langle p_T \rangle$	$\langle \theta \rangle$	$d^2\sigma/dpd\Omega$	$\langle p_T \rangle$	$\langle \theta \rangle$	$d^2\sigma/dpd\Omega$
0.36–0.42	0.389	67.5	$29.99 \pm 0.35 \pm 0.79$			
0.42–0.50	0.459	67.4	$26.77 \pm 0.29 \pm 0.70$	0.458	81.9	$19.01 \pm 0.25 \pm 0.63$
0.50–0.60	0.547	67.3	$19.65 \pm 0.23 \pm 0.70$	0.546	81.6	$12.23 \pm 0.18 \pm 0.54$
0.60–0.72	0.654	67.0	$11.87 \pm 0.17 \pm 0.62$	0.653	81.5	$6.04 \pm 0.13 \pm 0.41$
0.72–0.90	0.795	66.7	$5.58 \pm 0.10 \pm 0.42$	0.795	81.3	$2.42 \pm 0.07 \pm 0.24$
0.90–1.25	1.024	66.4	$1.34 \pm 0.04 \pm 0.18$	1.026	81.5	$0.56 \pm 0.02 \pm 0.09$
p_T	$90 < \theta < 105$			$105 < \theta < 125$		
	$\langle p_T \rangle$	$\langle \theta \rangle$	$d^2\sigma/dpd\Omega$	$\langle p_T \rangle$	$\langle \theta \rangle$	$d^2\sigma/dpd\Omega$
0.36–0.42				0.388	113.3	$7.21 \pm 0.15 \pm 0.27$
0.42–0.50	0.457	96.8	$10.65 \pm 0.18 \pm 0.52$	0.456	113.2	$4.82 \pm 0.11 \pm 0.23$
0.50–0.60	0.545	96.5	$6.21 \pm 0.13 \pm 0.37$	0.543	112.7	$2.28 \pm 0.07 \pm 0.18$
0.60–0.72	0.652	96.3	$2.57 \pm 0.08 \pm 0.22$	0.650	112.0	$0.75 \pm 0.04 \pm 0.09$
0.72–0.90	0.792	96.0	$0.91 \pm 0.04 \pm 0.10$	0.792	111.7	$0.21 \pm 0.02 \pm 0.04$
0.90–1.25	1.018	95.9	$0.19 \pm 0.02 \pm 0.04$	1.012	111.8	$0.03 \pm 0.01 \pm 0.02$

error on the proton energy loss in materials between the interaction vertex and the TPC volume leads to a momentum change larger than 2%. Pion cross-sections are not given if pions are separated from protons by less than twice the time-of-flight resolution.

The data given in Tables 2–10 are available in ASCII format in [21].

We refrain from presenting the wealth of cross-section data also in the form of plots. We limit ourselves to three representative figures that show the inclusive cross-sections of secondary protons, π^+'s, and π^-'s, produced by beams of protons, π^+'s, and π^-'s. We chose a polar-angle range that permits a good comparison of our results with published results from other experiments.

Table 3 Double-differential inclusive cross-section $d^2\sigma/dpd\Omega$ [mb/(GeV/c sr)] of the production of π^+'s in p + Be $\rightarrow \pi^+ +$ X interactions with +8.9 GeV/c beam momentum; the first error is statistical, the second systematic; p_T in GeV/c, polar angle θ in degrees

p_T	$20 < \theta < 30$			$30 < \theta < 40$		
	$\langle p_T \rangle$	$\langle \theta \rangle$	$d^2\sigma/dpd\Omega$	$\langle p_T \rangle$	$\langle \theta \rangle$	$d^2\sigma/dpd\Omega$
0.10–0.13	0.116	24.8	$53.94 \pm 1.04 \pm 3.98$	0.116	34.7	$37.12 \pm 0.84 \pm 2.54$
0.13–0.16	0.146	24.5	$68.32 \pm 1.08 \pm 3.91$	0.146	34.7	$48.46 \pm 0.92 \pm 2.53$
0.16–0.20	0.180	24.7	$80.65 \pm 0.98 \pm 3.65$	0.180	34.8	$51.60 \pm 0.78 \pm 2.26$
0.20–0.24	0.220	24.7	$83.11 \pm 0.98 \pm 3.08$	0.220	34.7	$55.60 \pm 0.80 \pm 2.10$
0.24–0.30	0.269	24.7	$76.59 \pm 0.76 \pm 2.44$	0.269	34.7	$51.20 \pm 0.61 \pm 1.60$
0.30–0.36	0.329	24.7	$63.92 \pm 0.69 \pm 1.83$	0.329	34.7	$43.01 \pm 0.56 \pm 1.19$
0.36–0.42	0.389	24.7	$51.22 \pm 0.61 \pm 1.46$	0.389	34.7	$35.38 \pm 0.51 \pm 0.96$
0.42–0.50	0.458	24.7	$39.63 \pm 0.46 \pm 1.35$	0.458	34.7	$27.21 \pm 0.38 \pm 0.83$
0.50–0.60	0.547	24.7	$24.72 \pm 0.31 \pm 1.18$	0.547	34.7	$17.24 \pm 0.27 \pm 0.72$
0.60–0.72	0.655	24.8	$14.28 \pm 0.21 \pm 1.02$	0.654	34.6	$9.97 \pm 0.18 \pm 0.62$
0.72–0.90				0.794	34.6	$4.41 \pm 0.09 \pm 0.44$
p_T	$40 < \theta < 50$			$50 < \theta < 60$		
	$\langle p_T \rangle$	$\langle \theta \rangle$	$d^2\sigma/dpd\Omega$	$\langle p_T \rangle$	$\langle \theta \rangle$	$d^2\sigma/dpd\Omega$
0.10–0.13	0.116	44.9	$28.16 \pm 0.73 \pm 1.94$			
0.13–0.16	0.145	44.9	$34.68 \pm 0.76 \pm 1.83$	0.146	54.9	$25.72 \pm 0.64 \pm 1.41$
0.16–0.20	0.180	44.8	$38.77 \pm 0.68 \pm 1.72$	0.180	54.8	$30.54 \pm 0.60 \pm 1.36$
0.20–0.24	0.220	44.7	$40.38 \pm 0.68 \pm 1.52$	0.220	54.8	$29.38 \pm 0.57 \pm 1.16$
0.24–0.30	0.269	44.7	$36.11 \pm 0.52 \pm 1.14$	0.269	54.7	$26.24 \pm 0.44 \pm 0.84$
0.30–0.36	0.329	44.8	$29.85 \pm 0.47 \pm 0.84$	0.329	54.7	$21.36 \pm 0.39 \pm 0.60$
0.36–0.42	0.389	44.7	$25.01 \pm 0.43 \pm 0.69$	0.389	54.8	$15.57 \pm 0.33 \pm 0.45$
0.42–0.50	0.458	44.6	$18.06 \pm 0.31 \pm 0.56$	0.457	54.7	$11.91 \pm 0.25 \pm 0.39$
0.50–0.60	0.547	44.6	$11.65 \pm 0.22 \pm 0.47$	0.546	54.6	$8.23 \pm 0.19 \pm 0.35$
0.60–0.72	0.655	44.6	$7.10 \pm 0.16 \pm 0.40$	0.654	54.7	$4.45 \pm 0.12 \pm 0.26$
0.72–0.90	0.795	44.5	$3.18 \pm 0.08 \pm 0.28$	0.793	54.3	$1.96 \pm 0.06 \pm 0.17$
0.90–1.25				1.027	54.2	$0.36 \pm 0.02 \pm 0.05$
p_T	$60 < \theta < 75$			$75 < \theta < 90$		
	$\langle p_T \rangle$	$\langle \theta \rangle$	$d^2\sigma/dpd\Omega$	$\langle p_T \rangle$	$\langle \theta \rangle$	$d^2\sigma/dpd\Omega$
0.13–0.16	0.146	67.1	$20.46 \pm 0.46 \pm 1.13$	0.145	82.5	$16.41 \pm 0.41 \pm 0.92$
0.16–0.20	0.180	67.3	$23.19 \pm 0.41 \pm 1.00$	0.180	82.2	$17.47 \pm 0.35 \pm 0.75$
0.20–0.24	0.219	67.2	$21.65 \pm 0.40 \pm 0.86$	0.219	82.0	$15.72 \pm 0.33 \pm 0.63$
0.24–0.30	0.269	67.0	$17.35 \pm 0.29 \pm 0.55$	0.268	82.0	$11.83 \pm 0.24 \pm 0.41$
0.30–0.36	0.329	66.9	$13.61 \pm 0.26 \pm 0.39$	0.328	81.9	$8.09 \pm 0.20 \pm 0.26$
0.36–0.42	0.388	66.8	$9.72 \pm 0.21 \pm 0.30$	0.388	81.9	$5.53 \pm 0.16 \pm 0.21$
0.42–0.50	0.457	66.7	$7.24 \pm 0.16 \pm 0.27$	0.458	81.9	$4.43 \pm 0.13 \pm 0.20$
0.50–0.60	0.546	66.7	$4.69 \pm 0.12 \pm 0.24$	0.543	81.9	$2.40 \pm 0.08 \pm 0.15$
0.60–0.72	0.653	66.3	$2.51 \pm 0.08 \pm 0.17$	0.654	81.3	$1.06 \pm 0.05 \pm 0.09$
0.72–0.90	0.792	66.4	$0.89 \pm 0.03 \pm 0.09$	0.791	81.3	$0.27 \pm 0.02 \pm 0.03$
0.90–1.25	1.010	66.0	$0.13 \pm 0.01 \pm 0.02$	1.002	81.4	$0.03 \pm 0.01 \pm 0.01$
p_T	$90 < \theta < 105$			$105 < \theta < 125$		
	$\langle p_T \rangle$	$\langle \theta \rangle$	$d^2\sigma/dpd\Omega$	$\langle p_T \rangle$	$\langle \theta \rangle$	$d^2\sigma/dpd\Omega$
0.13–0.16	0.145	97.4	$14.32 \pm 0.37 \pm 0.79$	0.145	114.9	$11.20 \pm 0.27 \pm 0.53$
0.16–0.20	0.179	97.3	$13.31 \pm 0.29 \pm 0.54$	0.179	114.0	$9.75 \pm 0.22 \pm 0.39$
0.20–0.24	0.219	97.2	$11.85 \pm 0.28 \pm 0.43$	0.219	113.7	$7.40 \pm 0.20 \pm 0.29$
0.24–0.30	0.268	96.9	$7.55 \pm 0.19 \pm 0.26$	0.267	113.6	$4.60 \pm 0.13 \pm 0.19$
0.30–0.36	0.328	96.8	$5.25 \pm 0.16 \pm 0.20$	0.327	113.6	$2.73 \pm 0.10 \pm 0.14$
0.36–0.42	0.387	96.6	$3.63 \pm 0.14 \pm 0.18$	0.387	113.2	$1.55 \pm 0.07 \pm 0.10$
0.42–0.50	0.457	96.4	$2.10 \pm 0.09 \pm 0.14$	0.455	112.8	$0.70 \pm 0.04 \pm 0.06$
0.50–0.60	0.541	96.2	$1.07 \pm 0.06 \pm 0.09$	0.536	111.5	$0.22 \pm 0.02 \pm 0.03$
0.60–0.72	0.650	95.9	$0.35 \pm 0.03 \pm 0.04$	0.655	111.2	$0.07 \pm 0.02 \pm 0.02$
0.72–0.90	0.788	95.5	$0.09 \pm 0.02 \pm 0.02$			

Table 4 Double-differential inclusive cross-section $d^2\sigma/dpd\Omega$ [mb/(GeV/c sr)] of the production of π^-'s in p + Be $\rightarrow \pi^-$ + X interactions with +8.9 GeV/c beam momentum; the first error is statistical, the second systematic; p_T in GeV/c, polar angle θ in degrees

p_T	$20 < \theta < 30$			$30 < \theta < 40$		
	$\langle p_T \rangle$	$\langle \theta \rangle$	$d^2\sigma/dpd\Omega$	$\langle p_T \rangle$	$\langle \theta \rangle$	$d^2\sigma/dpd\Omega$
0.10–0.13	0.116	24.7	$52.88 \pm 0.99 \pm 3.67$	0.116	34.7	$37.22 \pm 0.80 \pm 2.54$
0.13–0.16	0.145	24.8	$68.86 \pm 1.07 \pm 3.72$	0.145	34.7	$43.73 \pm 0.81 \pm 2.33$
0.16–0.20	0.180	24.7	$73.99 \pm 0.92 \pm 3.23$	0.180	34.7	$51.74 \pm 0.77 \pm 2.28$
0.20–0.24	0.220	24.8	$70.71 \pm 0.89 \pm 2.59$	0.220	34.6	$50.06 \pm 0.74 \pm 1.85$
0.24–0.30	0.269	24.8	$63.44 \pm 0.68 \pm 1.95$	0.269	34.7	$45.71 \pm 0.57 \pm 1.41$
0.30–0.36	0.329	24.8	$50.19 \pm 0.60 \pm 1.37$	0.329	34.8	$38.12 \pm 0.52 \pm 1.04$
0.36–0.42	0.389	24.8	$39.48 \pm 0.54 \pm 1.10$	0.389	34.7	$30.08 \pm 0.46 \pm 0.83$
0.42–0.50	0.458	24.8	$28.54 \pm 0.39 \pm 0.93$	0.457	34.7	$20.57 \pm 0.33 \pm 0.66$
0.50–0.60	0.545	24.8	$17.69 \pm 0.28 \pm 0.77$	0.545	34.8	$13.29 \pm 0.23 \pm 0.56$
0.60–0.72	0.654	24.9	$9.49 \pm 0.18 \pm 0.56$	0.653	34.8	$7.13 \pm 0.15 \pm 0.41$
0.72–0.90				0.792	35.0	$2.79 \pm 0.08 \pm 0.22$
p_T	$40 < \theta < 50$			$50 < \theta < 60$		
	$\langle p_T \rangle$	$\langle \theta \rangle$	$d^2\sigma/dpd\Omega$	$\langle p_T \rangle$	$\langle \theta \rangle$	$d^2\sigma/dpd\Omega$
0.10–0.13	0.116	44.9	$26.16 \pm 0.66 \pm 1.84$			
0.13–0.16	0.145	44.8	$32.69 \pm 0.70 \pm 1.74$	0.145	54.9	$27.00 \pm 0.62 \pm 1.51$
0.16–0.20	0.180	44.9	$35.72 \pm 0.63 \pm 1.58$	0.180	54.8	$30.60 \pm 0.58 \pm 1.38$
0.20–0.24	0.220	44.7	$35.26 \pm 0.61 \pm 1.32$	0.220	54.8	$29.13 \pm 0.57 \pm 1.10$
0.24–0.30	0.269	44.7	$31.62 \pm 0.47 \pm 0.98$	0.269	54.7	$24.82 \pm 0.43 \pm 0.77$
0.30–0.36	0.329	44.7	$27.66 \pm 0.45 \pm 0.76$	0.329	54.8	$18.64 \pm 0.36 \pm 0.52$
0.36–0.42	0.389	44.8	$20.94 \pm 0.38 \pm 0.60$	0.389	54.6	$14.03 \pm 0.30 \pm 0.42$
0.42–0.50	0.457	44.8	$14.98 \pm 0.27 \pm 0.50$	0.457	54.7	$10.00 \pm 0.22 \pm 0.35$
0.50–0.60	0.546	44.7	$8.98 \pm 0.18 \pm 0.40$	0.545	54.6	$6.11 \pm 0.15 \pm 0.28$
0.60–0.72	0.653	44.9	$5.38 \pm 0.13 \pm 0.33$	0.652	54.7	$3.33 \pm 0.10 \pm 0.21$
0.72–0.90	0.793	44.8	$1.79 \pm 0.06 \pm 0.15$	0.793	54.4	$1.35 \pm 0.05 \pm 0.12$
0.90–1.25				1.008	54.3	$0.23 \pm 0.02 \pm 0.03$
p_T	$60 < \theta < 75$			$75 < \theta < 90$		
	$\langle p_T \rangle$	$\langle \theta \rangle$	$d^2\sigma/dpd\Omega$	$\langle p_T \rangle$	$\langle \theta \rangle$	$d^2\sigma/dpd\Omega$
0.13–0.16	0.145	67.2	$21.82 \pm 0.46 \pm 1.18$	0.145	82.4	$15.38 \pm 0.37 \pm 0.86$
0.16–0.20	0.180	67.2	$22.68 \pm 0.39 \pm 0.95$	0.180	82.5	$16.85 \pm 0.32 \pm 0.69$
0.20–0.24	0.219	67.3	$21.05 \pm 0.38 \pm 0.76$	0.219	82.3	$15.18 \pm 0.32 \pm 0.55$
0.24–0.30	0.269	66.9	$15.96 \pm 0.27 \pm 0.47$	0.268	82.0	$10.95 \pm 0.22 \pm 0.33$
0.30–0.36	0.329	66.8	$12.48 \pm 0.23 \pm 0.36$	0.327	81.9	$7.40 \pm 0.18 \pm 0.24$
0.36–0.42	0.389	66.8	$9.45 \pm 0.20 \pm 0.30$	0.388	82.0	$4.85 \pm 0.14 \pm 0.19$
0.42–0.50	0.456	66.6	$6.04 \pm 0.13 \pm 0.24$	0.457	81.5	$3.58 \pm 0.11 \pm 0.18$
0.50–0.60	0.547	66.7	$3.85 \pm 0.10 \pm 0.20$	0.544	81.5	$1.82 \pm 0.07 \pm 0.12$
0.60–0.72	0.651	66.5	$1.73 \pm 0.06 \pm 0.12$	0.649	81.3	$0.97 \pm 0.05 \pm 0.09$
0.72–0.90	0.793	66.6	$0.69 \pm 0.03 \pm 0.07$	0.782	81.4	$0.25 \pm 0.02 \pm 0.03$
0.90–1.25	1.021	66.3	$0.10 \pm 0.01 \pm 0.02$	1.037	80.4	$0.04 \pm 0.01 \pm 0.01$
p_T	$90 < \theta < 105$			$105 < \theta < 125$		
	$\langle p_T \rangle$	$\langle \theta \rangle$	$d^2\sigma/dpd\Omega$	$\langle p_T \rangle$	$\langle \theta \rangle$	$d^2\sigma/dpd\Omega$
0.13–0.16	0.145	97.6	$15.03 \pm 0.36 \pm 0.83$	0.145	114.7	$11.38 \pm 0.26 \pm 0.53$
0.16–0.20	0.179	97.3	$14.31 \pm 0.30 \pm 0.57$	0.179	114.1	$9.10 \pm 0.19 \pm 0.32$
0.20–0.24	0.219	97.0	$11.02 \pm 0.25 \pm 0.39$	0.218	113.9	$6.71 \pm 0.17 \pm 0.24$
0.24–0.30	0.267	96.8	$7.66 \pm 0.18 \pm 0.25$	0.266	113.4	$3.92 \pm 0.11 \pm 0.17$
0.30–0.36	0.329	97.1	$4.97 \pm 0.15 \pm 0.20$	0.326	113.7	$2.45 \pm 0.09 \pm 0.14$
0.36–0.42	0.387	96.7	$2.91 \pm 0.11 \pm 0.16$	0.387	113.2	$1.44 \pm 0.07 \pm 0.11$
0.42–0.50	0.454	96.6	$1.88 \pm 0.08 \pm 0.13$	0.454	112.5	$0.70 \pm 0.04 \pm 0.07$
0.50–0.60	0.546	96.7	$0.82 \pm 0.05 \pm 0.08$	0.539	111.3	$0.22 \pm 0.02 \pm 0.03$
0.60–0.72	0.649	95.7	$0.33 \pm 0.03 \pm 0.04$	0.636	110.1	$0.05 \pm 0.01 \pm 0.02$
0.72–0.90	0.780	96.8	$0.08 \pm 0.02 \pm 0.02$			
0.90–1.25				1.020	114.1	$0.04 \pm 0.02 \pm 0.02$

Table 5 Double-differential inclusive cross-section $d^2\sigma/dpd\Omega$ [mb/(GeV/c sr)] of the production of protons in $\pi^+ + Be \to p + X$ interactions with +8.9 GeV/c beam momentum; the first error is statistical, the second systematic; p_T in GeV/c, polar angle θ in degrees

p_T	$20 < \theta < 30$			$30 < \theta < 40$		
	$\langle p_T \rangle$	$\langle \theta \rangle$	$d^2\sigma/dpd\Omega$	$\langle p_T \rangle$	$\langle \theta \rangle$	$d^2\sigma/dpd\Omega$
0.20–0.24	0.220	24.8	$34.44 \pm 0.76 \pm 1.62$			
0.24–0.30	0.269	25.1	$36.77 \pm 0.64 \pm 1.54$	0.270	34.9	$32.90 \pm 0.66 \pm 1.30$
0.30–0.36	0.329	25.0	$32.47 \pm 0.58 \pm 1.22$	0.330	34.9	$30.81 \pm 0.56 \pm 1.07$
0.36–0.42	0.389	24.9	$30.62 \pm 0.56 \pm 1.05$	0.389	34.9	$27.98 \pm 0.54 \pm 0.89$
0.42–0.50	0.458	25.0	$28.19 \pm 0.47 \pm 0.90$	0.459	34.9	$25.72 \pm 0.45 \pm 0.78$
0.50–0.60	0.547	24.9	$23.47 \pm 0.37 \pm 0.77$	0.548	34.9	$20.87 \pm 0.36 \pm 0.65$
0.60–0.72	0.656	24.9	$19.42 \pm 0.31 \pm 0.74$	0.657	34.8	$15.84 \pm 0.28 \pm 0.59$
0.72–0.90				0.802	34.8	$10.53 \pm 0.19 \pm 0.54$
p_T	$40 < \theta < 50$			$50 < \theta < 60$		
	$\langle p_T \rangle$	$\langle \theta \rangle$	$d^2\sigma/dpd\Omega$	$\langle p_T \rangle$	$\langle \theta \rangle$	$d^2\sigma/dpd\Omega$
0.30–0.36	0.330	45.0	$30.20 \pm 0.55 \pm 1.00$			
0.36–0.42	0.389	45.0	$28.76 \pm 0.55 \pm 0.85$	0.389	55.0	$26.46 \pm 0.51 \pm 0.75$
0.42–0.50	0.459	45.0	$23.87 \pm 0.44 \pm 0.69$	0.458	54.8	$20.94 \pm 0.40 \pm 0.61$
0.50–0.60	0.548	44.9	$17.94 \pm 0.34 \pm 0.58$	0.547	54.9	$15.89 \pm 0.32 \pm 0.55$
0.60–0.72	0.656	44.8	$13.30 \pm 0.27 \pm 0.51$	0.657	54.9	$11.27 \pm 0.26 \pm 0.48$
0.72–0.90	0.800	44.9	$8.01 \pm 0.18 \pm 0.42$	0.799	54.8	$5.75 \pm 0.15 \pm 0.33$
0.90–1.25	1.031	44.7	$2.74 \pm 0.07 \pm 0.22$	1.027	54.8	$1.69 \pm 0.06 \pm 0.15$
p_T	$60 < \theta < 75$			$75 < \theta < 90$		
	$\langle p_T \rangle$	$\langle \theta \rangle$	$d^2\sigma/dpd\Omega$	$\langle p_T \rangle$	$\langle \theta \rangle$	$d^2\sigma/dpd\Omega$
0.36–0.42	0.389	67.4	$22.14 \pm 0.37 \pm 0.72$			
0.42–0.50	0.458	67.3	$20.09 \pm 0.32 \pm 0.58$	0.457	81.9	$14.52 \pm 0.27 \pm 0.53$
0.50–0.60	0.547	67.2	$14.32 \pm 0.25 \pm 0.51$	0.545	81.8	$9.33 \pm 0.20 \pm 0.42$
0.60–0.72	0.655	67.2	$8.69 \pm 0.18 \pm 0.44$	0.654	81.7	$4.55 \pm 0.13 \pm 0.30$
0.72–0.90	0.796	66.7	$4.07 \pm 0.10 \pm 0.29$	0.798	81.5	$2.00 \pm 0.07 \pm 0.18$
0.90–1.25	1.026	66.3	$0.96 \pm 0.04 \pm 0.11$	1.018	81.5	$0.47 \pm 0.03 \pm 0.06$
p_T	$90 < \theta < 105$			$105 < \theta < 125$		
	$\langle p_T \rangle$	$\langle \theta \rangle$	$d^2\sigma/dpd\Omega$	$\langle p_T \rangle$	$\langle \theta \rangle$	$d^2\sigma/dpd\Omega$
0.36–0.42				0.388	113.7	$6.70 \pm 0.18 \pm 0.24$
0.42–0.50	0.456	96.9	$8.60 \pm 0.21 \pm 0.41$	0.457	113.5	$4.45 \pm 0.13 \pm 0.20$
0.50–0.60	0.545	96.7	$5.17 \pm 0.15 \pm 0.31$	0.544	112.8	$2.26 \pm 0.09 \pm 0.17$
0.60–0.72	0.650	96.6	$2.26 \pm 0.10 \pm 0.18$	0.647	112.7	$0.71 \pm 0.05 \pm 0.08$
0.72–0.90	0.792	96.4	$0.76 \pm 0.05 \pm 0.08$	0.793	112.1	$0.22 \pm 0.02 \pm 0.04$
0.90–1.25	1.018	95.8	$0.19 \pm 0.02 \pm 0.03$	1.016	111.6	$0.03 \pm 0.01 \pm 0.01$

Figure 13 illustrates our measurement of the inclusive cross-sections $d^2\sigma/dpd\Omega$ of proton and $\pi^\pm$ production by +8.9 GeV/c incoming protons, in the polar angle range $20° < \theta < 30°$.

Figure 14 illustrates our measurement of the inclusive cross-sections $d^2\sigma/dpd\Omega$ of proton and $\pi^\pm$ production by +8.9 GeV/c incoming π^+'s, in the polar angle range $20° < \theta < 30°$.

Figure 15 illustrates our measurement of the inclusive cross-sections $d^2\sigma/dpd\Omega$ of proton and $\pi^\pm$ production by −8.0 GeV/c incoming π^-'s, in the polar angle range $20° < \theta < 30°$.

9 Comparison with other experimental results

We compare our +8.9 GeV/c Be cross-sections with those from other experiments and with the results obtained by the HARP Collaboration from the same data that we analysed. The data of the other experiments are from E802 and E910

Table 6 Double-differential inclusive cross-section $\mathrm{d}^2\sigma/\mathrm{d}p\mathrm{d}\Omega$ [mb/(GeV/c sr)] of the production of π^+'s in $\pi^+ + \mathrm{Be} \to \pi^+ + \mathrm{X}$ interactions with +8.9 GeV/c beam momentum; the first error is statistical, the second systematic; p_T in GeV/c, polar angle θ in degrees

p_T	$20 < \theta < 30$			$30 < \theta < 40$		
	$\langle p_\mathrm{T}\rangle$	$\langle\theta\rangle$	$\mathrm{d}^2\sigma/\mathrm{d}p\mathrm{d}\Omega$	$\langle p_\mathrm{T}\rangle$	$\langle\theta\rangle$	$\mathrm{d}^2\sigma/\mathrm{d}p\mathrm{d}\Omega$
0.10–0.13	0.115	24.6	$52.73 \pm 1.28 \pm 3.46$	0.116	34.7	$38.43 \pm 1.06 \pm 2.58$
0.13–0.16	0.145	24.6	$68.39 \pm 1.35 \pm 3.63$	0.146	34.7	$49.02 \pm 1.16 \pm 2.55$
0.16–0.20	0.180	24.6	$85.35 \pm 1.26 \pm 3.81$	0.180	34.7	$54.25 \pm 0.99 \pm 2.36$
0.20–0.24	0.220	24.7	$90.83 \pm 1.28 \pm 3.47$	0.220	34.7	$59.18 \pm 1.03 \pm 2.21$
0.24–0.30	0.270	24.6	$86.94 \pm 1.01 \pm 2.86$	0.270	34.7	$55.39 \pm 0.80 \pm 1.77$
0.30–0.36	0.329	24.7	$78.97 \pm 0.96 \pm 2.38$	0.329	34.6	$49.51 \pm 0.75 \pm 1.41$
0.36–0.42	0.389	24.6	$65.31 \pm 0.86 \pm 1.97$	0.389	34.5	$41.04 \pm 0.68 \pm 1.14$
0.42–0.50	0.458	24.6	$50.82 \pm 0.66 \pm 1.77$	0.458	34.7	$31.00 \pm 0.51 \pm 0.97$
0.50–0.60	0.546	24.6	$34.19 \pm 0.47 \pm 1.65$	0.546	34.6	$20.89 \pm 0.37 \pm 0.89$
0.60–0.72	0.653	24.5	$20.15 \pm 0.32 \pm 1.44$	0.655	34.6	$12.10 \pm 0.25 \pm 0.76$
0.72–0.90				0.796	34.4	$5.44 \pm 0.13 \pm 0.55$
p_T	$40 < \theta < 50$			$50 < \theta < 60$		
	$\langle p_\mathrm{T}\rangle$	$\langle\theta\rangle$	$\mathrm{d}^2\sigma/\mathrm{d}p\mathrm{d}\Omega$	$\langle p_\mathrm{T}\rangle$	$\langle\theta\rangle$	$\mathrm{d}^2\sigma/\mathrm{d}p\mathrm{d}\Omega$
0.10–0.13	0.116	44.8	$27.23 \pm 0.89 \pm 1.89$			
0.13–0.16	0.145	45.0	$34.43 \pm 0.95 \pm 1.80$	0.146	54.8	$26.57 \pm 0.81 \pm 1.47$
0.16–0.20	0.180	44.7	$40.25 \pm 0.86 \pm 1.76$	0.180	54.8	$29.74 \pm 0.74 \pm 1.31$
0.20–0.24	0.220	44.7	$41.13 \pm 0.86 \pm 1.55$	0.220	54.7	$29.17 \pm 0.72 \pm 1.09$
0.24–0.30	0.269	44.8	$37.59 \pm 0.66 \pm 1.21$	0.269	54.7	$27.17 \pm 0.56 \pm 0.86$
0.30–0.36	0.329	44.7	$31.47 \pm 0.60 \pm 0.91$	0.329	54.6	$22.68 \pm 0.51 \pm 0.66$
0.36–0.42	0.389	44.6	$26.25 \pm 0.55 \pm 0.75$	0.388	54.6	$16.42 \pm 0.42 \pm 0.49$
0.42–0.50	0.458	44.6	$19.54 \pm 0.41 \pm 0.62$	0.457	54.7	$13.11 \pm 0.33 \pm 0.44$
0.50–0.60	0.545	44.6	$13.17 \pm 0.29 \pm 0.53$	0.547	54.6	$8.35 \pm 0.23 \pm 0.36$
0.60–0.72	0.654	44.4	$7.69 \pm 0.20 \pm 0.44$	0.654	54.5	$5.26 \pm 0.17 \pm 0.31$
0.72–0.90	0.793	44.5	$3.72 \pm 0.11 \pm 0.32$	0.791	54.4	$2.28 \pm 0.09 \pm 0.19$
0.90–1.25				1.012	54.3	$0.38 \pm 0.02 \pm 0.06$
p_T	$60 < \theta < 75$			$75 < \theta < 90$		
	$\langle p_\mathrm{T}\rangle$	$\langle\theta\rangle$	$\mathrm{d}^2\sigma/\mathrm{d}p\mathrm{d}\Omega$	$\langle p_\mathrm{T}\rangle$	$\langle\theta\rangle$	$\mathrm{d}^2\sigma/\mathrm{d}p\mathrm{d}\Omega$
0.13–0.16	0.146	67.4	$19.92 \pm 0.56 \pm 1.14$	0.146	82.6	$16.19 \pm 0.51 \pm 1.00$
0.16–0.20	0.180	67.2	$21.98 \pm 0.50 \pm 0.97$	0.180	82.2	$17.37 \pm 0.44 \pm 0.81$
0.20–0.24	0.219	66.9	$21.74 \pm 0.50 \pm 0.80$	0.219	82.2	$16.33 \pm 0.43 \pm 0.59$
0.24–0.30	0.269	67.2	$18.47 \pm 0.38 \pm 0.57$	0.268	81.9	$11.54 \pm 0.29 \pm 0.35$
0.30–0.36	0.329	66.8	$14.14 \pm 0.33 \pm 0.41$	0.328	82.1	$8.72 \pm 0.26 \pm 0.27$
0.36–0.42	0.389	66.7	$10.89 \pm 0.28 \pm 0.34$	0.389	81.9	$5.93 \pm 0.20 \pm 0.22$
0.42–0.50	0.457	66.7	$7.65 \pm 0.20 \pm 0.30$	0.458	81.8	$4.88 \pm 0.17 \pm 0.23$
0.50–0.60	0.545	66.6	$5.50 \pm 0.16 \pm 0.28$	0.546	81.8	$2.80 \pm 0.11 \pm 0.17$
0.60–0.72	0.654	66.3	$2.95 \pm 0.11 \pm 0.20$	0.653	81.7	$1.30 \pm 0.07 \pm 0.11$
0.72–0.90	0.794	66.2	$1.03 \pm 0.05 \pm 0.10$	0.785	81.0	$0.43 \pm 0.03 \pm 0.05$
0.90–1.25	1.021	65.7	$0.16 \pm 0.02 \pm 0.03$	1.007	81.2	$0.05 \pm 0.01 \pm 0.01$
p_T	$90 < \theta < 105$			$105 < \theta < 125$		
	$\langle p_\mathrm{T}\rangle$	$\langle\theta\rangle$	$\mathrm{d}^2\sigma/\mathrm{d}p\mathrm{d}\Omega$	$\langle p_\mathrm{T}\rangle$	$\langle\theta\rangle$	$\mathrm{d}^2\sigma/\mathrm{d}p\mathrm{d}\Omega$
0.13–0.16	0.145	97.1	$13.79 \pm 0.46 \pm 0.85$	0.145	114.8	$10.53 \pm 0.33 \pm 0.66$
0.16–0.20	0.179	97.3	$12.92 \pm 0.36 \pm 0.60$	0.179	114.5	$9.68 \pm 0.27 \pm 0.48$
0.20–0.24	0.219	97.2	$11.60 \pm 0.35 \pm 0.42$	0.219	114.0	$7.56 \pm 0.25 \pm 0.27$
0.24–0.30	0.267	97.0	$8.27 \pm 0.25 \pm 0.27$	0.267	113.5	$5.03 \pm 0.17 \pm 0.19$
0.30–0.36	0.328	96.9	$5.50 \pm 0.20 \pm 0.21$	0.327	113.7	$2.86 \pm 0.13 \pm 0.15$
0.36–0.42	0.389	97.1	$4.23 \pm 0.18 \pm 0.21$	0.387	113.6	$1.71 \pm 0.10 \pm 0.12$
0.42–0.50	0.457	96.7	$2.37 \pm 0.11 \pm 0.15$	0.457	112.4	$0.94 \pm 0.06 \pm 0.08$
0.50–0.60	0.539	96.1	$1.34 \pm 0.08 \pm 0.12$	0.541	111.9	$0.31 \pm 0.03 \pm 0.04$
0.60–0.72	0.652	96.3	$0.45 \pm 0.04 \pm 0.05$	0.650	111.9	$0.12 \pm 0.02 \pm 0.02$
0.72–0.90	0.794	95.5	$0.10 \pm 0.02 \pm 0.02$			

Table 7 Double-differential inclusive cross-section $\mathrm{d}^2\sigma/\mathrm{d}p\mathrm{d}\Omega$ [mb/(GeV/c sr)] of the production of π^-'s in $\pi^+ + \mathrm{Be} \to \pi^- + \mathrm{X}$ interactions with +8.9 GeV/c beam momentum; the first error is statistical, the second systematic; p_T in GeV/c, polar angle θ in degrees

p_T	$20 < \theta < 30$			$30 < \theta < 40$		
	$\langle p_\mathrm{T}\rangle$	$\langle\theta\rangle$	$\mathrm{d}^2\sigma/\mathrm{d}p\mathrm{d}\Omega$	$\langle p_\mathrm{T}\rangle$	$\langle\theta\rangle$	$\mathrm{d}^2\sigma/\mathrm{d}p\mathrm{d}\Omega$
0.10–0.13	0.116	24.8	$46.25 \pm 1.15 \pm 3.10$	0.116	34.8	$33.42 \pm 0.94 \pm 2.33$
0.13–0.16	0.146	24.6	$61.24 \pm 1.26 \pm 3.17$	0.145	34.6	$36.42 \pm 0.92 \pm 1.93$
0.16–0.20	0.180	24.7	$65.33 \pm 1.07 \pm 2.89$	0.180	34.6	$43.91 \pm 0.88 \pm 1.95$
0.20–0.24	0.220	24.6	$70.02 \pm 1.10 \pm 2.61$	0.220	34.6	$44.85 \pm 0.87 \pm 1.69$
0.24–0.30	0.269	24.7	$63.57 \pm 0.85 \pm 2.03$	0.270	34.7	$42.49 \pm 0.69 \pm 1.35$
0.30–0.36	0.329	24.7	$51.65 \pm 0.76 \pm 1.45$	0.329	34.7	$35.06 \pm 0.62 \pm 0.99$
0.36–0.42	0.388	24.7	$42.11 \pm 0.69 \pm 1.20$	0.389	34.6	$28.74 \pm 0.56 \pm 0.81$
0.42–0.50	0.457	24.7	$31.10 \pm 0.51 \pm 1.03$	0.458	34.7	$19.88 \pm 0.40 \pm 0.65$
0.50–0.60	0.546	24.7	$19.63 \pm 0.36 \pm 0.86$	0.546	34.8	$12.89 \pm 0.29 \pm 0.55$
0.60–0.72	0.652	24.6	$10.21 \pm 0.23 \pm 0.61$	0.652	34.8	$6.87 \pm 0.19 \pm 0.41$
0.72–0.90				0.793	34.7	$2.89 \pm 0.10 \pm 0.24$
p_T	$40 < \theta < 50$			$50 < \theta < 60$		
	$\langle p_\mathrm{T}\rangle$	$\langle\theta\rangle$	$\mathrm{d}^2\sigma/\mathrm{d}p\mathrm{d}\Omega$	$\langle p_\mathrm{T}\rangle$	$\langle\theta\rangle$	$\mathrm{d}^2\sigma/\mathrm{d}p\mathrm{d}\Omega$
0.10–0.13	0.116	44.7	$22.32 \pm 0.76 \pm 1.63$			
0.13–0.16	0.145	44.8	$26.81 \pm 0.79 \pm 1.48$	0.145	54.9	$20.72 \pm 0.68 \pm 1.34$
0.16–0.20	0.180	44.7	$30.04 \pm 0.72 \pm 1.35$	0.181	54.8	$23.25 \pm 0.63 \pm 1.07$
0.20–0.24	0.220	44.7	$29.53 \pm 0.70 \pm 1.14$	0.220	54.7	$24.07 \pm 0.64 \pm 0.92$
0.24–0.30	0.270	44.7	$27.50 \pm 0.55 \pm 0.88$	0.269	54.8	$20.77 \pm 0.49 \pm 0.66$
0.30–0.36	0.329	44.8	$24.30 \pm 0.52 \pm 0.69$	0.329	54.6	$16.27 \pm 0.41 \pm 0.49$
0.36–0.42	0.389	44.8	$18.89 \pm 0.45 \pm 0.56$	0.388	54.7	$11.66 \pm 0.34 \pm 0.36$
0.42–0.50	0.458	44.7	$13.59 \pm 0.33 \pm 0.47$	0.457	54.7	$9.07 \pm 0.26 \pm 0.37$
0.50–0.60	0.544	44.9	$8.19 \pm 0.22 \pm 0.38$	0.546	54.8	$5.79 \pm 0.18 \pm 0.30$
0.60–0.72	0.652	44.7	$4.95 \pm 0.16 \pm 0.32$	0.653	54.6	$2.94 \pm 0.12 \pm 0.20$
0.72–0.90	0.797	44.7	$1.74 \pm 0.07 \pm 0.16$	0.793	54.6	$1.29 \pm 0.07 \pm 0.12$
0.90–1.25				1.020	54.4	$0.20 \pm 0.02 \pm 0.03$
p_T	$60 < \theta < 75$			$75 < \theta < 90$		
	$\langle p_\mathrm{T}\rangle$	$\langle\theta\rangle$	$\mathrm{d}^2\sigma/\mathrm{d}p\mathrm{d}\Omega$	$\langle p_\mathrm{T}\rangle$	$\langle\theta\rangle$	$\mathrm{d}^2\sigma/\mathrm{d}p\mathrm{d}\Omega$
0.13–0.16	0.145	67.2	$16.30 \pm 0.50 \pm 0.98$	0.145	82.3	$11.29 \pm 0.39 \pm 0.78$
0.16–0.20	0.180	67.4	$17.40 \pm 0.43 \pm 0.81$	0.180	82.3	$12.37 \pm 0.35 \pm 0.65$
0.20–0.24	0.220	67.2	$16.22 \pm 0.42 \pm 0.58$	0.220	82.4	$11.29 \pm 0.34 \pm 0.48$
0.24–0.30	0.269	67.0	$13.86 \pm 0.31 \pm 0.42$	0.268	82.0	$8.66 \pm 0.24 \pm 0.29$
0.30–0.36	0.329	66.9	$10.08 \pm 0.26 \pm 0.31$	0.328	81.8	$5.91 \pm 0.20 \pm 0.24$
0.36–0.42	0.388	66.8	$8.08 \pm 0.23 \pm 0.32$	0.388	82.0	$4.51 \pm 0.17 \pm 0.20$
0.42–0.50	0.458	66.7	$5.41 \pm 0.16 \pm 0.25$	0.456	81.6	$3.29 \pm 0.13 \pm 0.18$
0.50–0.60	0.546	66.7	$3.23 \pm 0.11 \pm 0.19$	0.543	81.3	$1.79 \pm 0.08 \pm 0.13$
0.60–0.72	0.654	66.2	$1.60 \pm 0.07 \pm 0.12$	0.652	81.2	$0.88 \pm 0.06 \pm 0.08$
0.72–0.90	0.790	66.4	$0.74 \pm 0.04 \pm 0.08$	0.786	81.0	$0.30 \pm 0.02 \pm 0.04$
0.90–1.25	1.017	66.2	$0.12 \pm 0.01 \pm 0.02$	1.004	81.4	$0.04 \pm 0.01 \pm 0.01$
p_T	$90 < \theta < 105$			$105 < \theta < 125$		
	$\langle p_\mathrm{T}\rangle$	$\langle\theta\rangle$	$\mathrm{d}^2\sigma/\mathrm{d}p\mathrm{d}\Omega$	$\langle p_\mathrm{T}\rangle$	$\langle\theta\rangle$	$\mathrm{d}^2\sigma/\mathrm{d}p\mathrm{d}\Omega$
0.13–0.16	0.145	97.3	$10.63 \pm 0.38 \pm 0.77$	0.145	114.9	$8.61 \pm 0.28 \pm 0.72$
0.16–0.20	0.179	97.1	$10.19 \pm 0.31 \pm 0.63$	0.179	114.0	$6.45 \pm 0.20 \pm 0.44$
0.20–0.24	0.219	97.0	$7.74 \pm 0.26 \pm 0.43$	0.218	113.6	$5.65 \pm 0.20 \pm 0.28$
0.24–0.30	0.267	97.0	$6.15 \pm 0.20 \pm 0.27$	0.267	113.8	$3.38 \pm 0.13 \pm 0.16$
0.30–0.36	0.328	97.0	$4.37 \pm 0.17 \pm 0.19$	0.326	113.3	$2.20 \pm 0.11 \pm 0.13$
0.36–0.42	0.388	96.7	$2.61 \pm 0.13 \pm 0.16$	0.390	112.9	$1.27 \pm 0.08 \pm 0.10$
0.42–0.50	0.457	96.8	$1.65 \pm 0.09 \pm 0.12$	0.454	113.6	$0.74 \pm 0.05 \pm 0.07$
0.50–0.60	0.543	96.7	$0.89 \pm 0.06 \pm 0.09$	0.540	111.9	$0.24 \pm 0.03 \pm 0.03$
0.60–0.72	0.649	95.8	$0.38 \pm 0.04 \pm 0.05$	0.656	111.2	$0.09 \pm 0.02 \pm 0.02$
0.72–0.90	0.791	96.2	$0.07 \pm 0.02 \pm 0.02$			

Table 8 Double-differential inclusive cross-section $d^2\sigma/dpd\Omega$ [mb/(GeV/c sr)] of the production of protons in $\pi^- + \text{Be} \to \text{p} + \text{X}$ interactions with −8.0 GeV/c beam momentum; the first error is statistical, the second systematic; p_T in GeV/c, polar angle θ in degrees

p_T	$20 < \theta < 30$			$30 < \theta < 40$		
	$\langle p_T \rangle$	$\langle \theta \rangle$	$d^2\sigma/dpd\Omega$	$\langle p_T \rangle$	$\langle \theta \rangle$	$d^2\sigma/dpd\Omega$
0.20–0.24	0.221	25.1	$28.46 \pm 1.02 \pm 1.39$			
0.24–0.30	0.269	25.0	$26.71 \pm 0.79 \pm 1.15$	0.271	35.0	$26.35 \pm 0.77 \pm 1.07$
0.30–0.36	0.329	24.9	$27.13 \pm 0.79 \pm 1.06$	0.330	34.9	$25.06 \pm 0.75 \pm 0.93$
0.36–0.42	0.389	25.0	$24.92 \pm 0.76 \pm 0.89$	0.389	35.0	$23.28 \pm 0.73 \pm 0.79$
0.42–0.50	0.459	25.0	$22.28 \pm 0.60 \pm 0.73$	0.459	35.0	$17.73 \pm 0.55 \pm 0.57$
0.50–0.60	0.547	24.9	$19.55 \pm 0.50 \pm 0.65$	0.548	34.8	$16.55 \pm 0.48 \pm 0.54$
0.60–0.72	0.658	24.9	$14.55 \pm 0.40 \pm 0.57$	0.656	34.8	$12.50 \pm 0.38 \pm 0.49$
0.72–0.90				0.801	34.9	$7.74 \pm 0.24 \pm 0.40$
p_T	$40 < \theta < 50$			$50 < \theta < 60$		
	$\langle p_T \rangle$	$\langle \theta \rangle$	$d^2\sigma/dpd\Omega$	$\langle p_T \rangle$	$\langle \theta \rangle$	$d^2\sigma/dpd\Omega$
0.30–0.36	0.329	45.0	$24.35 \pm 0.73 \pm 0.82$			
0.36–0.42	0.389	44.9	$20.62 \pm 0.67 \pm 0.63$	0.389	54.9	$20.67 \pm 0.67 \pm 0.65$
0.42–0.50	0.457	45.0	$18.61 \pm 0.56 \pm 0.57$	0.458	55.0	$16.70 \pm 0.52 \pm 0.53$
0.50–0.60	0.547	44.8	$14.12 \pm 0.45 \pm 0.47$	0.548	55.0	$12.55 \pm 0.43 \pm 0.46$
0.60–0.72	0.656	44.9	$9.24 \pm 0.33 \pm 0.37$	0.655	54.9	$8.68 \pm 0.33 \pm 0.38$
0.72–0.90	0.799	45.0	$6.23 \pm 0.23 \pm 0.34$	0.800	55.0	$4.79 \pm 0.20 \pm 0.28$
0.90–1.25	1.046	44.9	$1.78 \pm 0.09 \pm 0.15$	1.044	54.9	$1.37 \pm 0.08 \pm 0.13$
p_T	$60 < \theta < 75$			$75 < \theta < 90$		
	$\langle p_T \rangle$	$\langle \theta \rangle$	$d^2\sigma/dpd\Omega$	$\langle p_T \rangle$	$\langle \theta \rangle$	$d^2\sigma/dpd\Omega$
0.36–0.42	0.389	67.5	$18.23 \pm 0.50 \pm 0.61$			
0.42–0.50	0.458	67.4	$16.13 \pm 0.42 \pm 0.47$	0.458	81.7	$10.95 \pm 0.34 \pm 0.42$
0.50–0.60	0.546	67.4	$11.55 \pm 0.33 \pm 0.43$	0.546	81.7	$7.54 \pm 0.26 \pm 0.34$
0.60–0.72	0.654	67.2	$6.82 \pm 0.24 \pm 0.36$	0.655	81.7	$3.88 \pm 0.18 \pm 0.27$
0.72–0.90	0.797	67.2	$3.50 \pm 0.15 \pm 0.27$	0.796	81.7	$1.69 \pm 0.10 \pm 0.15$
0.90–1.25	1.038	66.7	$0.78 \pm 0.05 \pm 0.10$	1.024	81.7	$0.44 \pm 0.04 \pm 0.06$
p_T	$90 < \theta < 105$			$105 < \theta < 125$		
	$\langle p_T \rangle$	$\langle \theta \rangle$	$d^2\sigma/dpd\Omega$	$\langle p_T \rangle$	$\langle \theta \rangle$	$d^2\sigma/dpd\Omega$
0.36–0.42				0.388	113.6	$4.91 \pm 0.23 \pm 0.19$
0.42–0.50	0.457	96.6	$6.78 \pm 0.27 \pm 0.34$	0.456	113.6	$3.32 \pm 0.16 \pm 0.16$
0.50–0.60	0.545	96.7	$4.23 \pm 0.20 \pm 0.26$	0.541	113.0	$1.88 \pm 0.12 \pm 0.15$
0.60–0.72	0.657	96.5	$2.04 \pm 0.14 \pm 0.17$	0.654	113.2	$0.79 \pm 0.07 \pm 0.10$
0.72–0.90	0.795	96.6	$0.79 \pm 0.07 \pm 0.08$	0.792	111.9	$0.29 \pm 0.04 \pm 0.05$
0.90–1.25	1.018	96.1	$0.23 \pm 0.03 \pm 0.03$	1.035	111.8	$0.05 \pm 0.02 \pm 0.02$

which were obtained with somewhat higher beam momenta. A more direct comparison with these data will be given in a forthcoming paper [22] where we present cross-sections on Be for all beam momenta from 3 GeV/c to 15 GeV/c.

9.1 Comparison with E802 results

Experiment E802 [23] at Brookhaven National Laboratory measured secondary π^+'s in the polar-angle range $5° < \theta < 58°$ from the interactions of 14.6 GeV/c protons with beryllium nuclei.

Figure 16 shows their published Lorentz-invariant cross-section of π^+ and π^- production by 14.6 GeV/c protons, in the rapidity range $1.2 < y < 1.4$, as a function of $m_T - m_\pi$, where m_T denotes the transverse mass. Their data are compared with our results expressed in the same units as used by E802.

Table 9 Double-differential inclusive cross-section $\mathrm{d}^2\sigma/\mathrm{d}p\mathrm{d}\Omega$ [mb/(GeV/c sr)] of the production of π^+'s in $\pi^- + \mathrm{Be} \to \pi^+ + \mathrm{X}$ interactions with -8.0 GeV/c beam momentum; the first error is statistical, the second systematic; p_T in GeV/c, polar angle θ in degrees

p_T	$20 < \theta < 30$			$30 < \theta < 40$		
	$\langle p_\mathrm{T}\rangle$	$\langle\theta\rangle$	$\mathrm{d}^2\sigma/\mathrm{d}p\mathrm{d}\Omega$	$\langle p_\mathrm{T}\rangle$	$\langle\theta\rangle$	$\mathrm{d}^2\sigma/\mathrm{d}p\mathrm{d}\Omega$
0.10–0.13	0.116	24.5	$40.03 \pm 1.60 \pm 2.82$	0.116	34.7	$27.55 \pm 1.32 \pm 1.90$
0.13–0.16	0.146	24.6	$51.88 \pm 1.74 \pm 2.87$	0.145	34.8	$38.40 \pm 1.48 \pm 2.07$
0.16–0.20	0.181	24.5	$58.09 \pm 1.48 \pm 2.61$	0.181	34.8	$40.43 \pm 1.25 \pm 1.79$
0.20–0.24	0.220	24.6	$61.57 \pm 1.52 \pm 2.38$	0.220	34.6	$41.25 \pm 1.23 \pm 1.59$
0.24–0.30	0.270	24.7	$58.68 \pm 1.19 \pm 1.94$	0.269	34.7	$43.31 \pm 1.02 \pm 1.42$
0.30–0.36	0.328	24.6	$53.20 \pm 1.14 \pm 1.58$	0.329	34.8	$36.40 \pm 0.94 \pm 1.07$
0.36–0.42	0.389	24.6	$41.85 \pm 0.99 \pm 1.35$	0.389	34.7	$28.53 \pm 0.82 \pm 0.83$
0.42–0.50	0.457	24.6	$31.72 \pm 0.74 \pm 1.11$	0.457	34.6	$19.60 \pm 0.58 \pm 0.63$
0.50–0.60	0.545	24.7	$21.39 \pm 0.53 \pm 1.04$	0.545	34.8	$12.58 \pm 0.40 \pm 0.55$
0.60–0.72	0.655	24.7	$11.72 \pm 0.34 \pm 0.84$	0.656	34.7	$7.16 \pm 0.26 \pm 0.46$
0.72–0.90				0.796	34.5	$2.87 \pm 0.12 \pm 0.30$
p_T	$40 < \theta < 50$			$50 < \theta < 60$		
	$\langle p_\mathrm{T}\rangle$	$\langle\theta\rangle$	$\mathrm{d}^2\sigma/\mathrm{d}p\mathrm{d}\Omega$	$\langle p_\mathrm{T}\rangle$	$\langle\theta\rangle$	$\mathrm{d}^2\sigma/\mathrm{d}p\mathrm{d}\Omega$
0.10–0.13	0.117	45.0	$21.40 \pm 1.17 \pm 1.54$			
0.13–0.16	0.146	44.9	$25.24 \pm 1.15 \pm 1.38$	0.146	54.9	$19.22 \pm 0.99 \pm 1.14$
0.16–0.20	0.179	44.8	$29.56 \pm 1.07 \pm 1.34$	0.180	54.8	$21.66 \pm 0.90 \pm 0.99$
0.20–0.24	0.220	44.9	$29.03 \pm 1.03 \pm 1.14$	0.220	54.7	$22.20 \pm 0.92 \pm 0.87$
0.24–0.30	0.270	44.7	$26.44 \pm 0.80 \pm 0.88$	0.269	54.9	$20.48 \pm 0.71 \pm 0.68$
0.30–0.36	0.329	44.7	$23.88 \pm 0.76 \pm 0.72$	0.329	54.7	$16.76 \pm 0.62 \pm 0.51$
0.36–0.42	0.388	44.7	$18.64 \pm 0.66 \pm 0.56$	0.389	54.8	$14.55 \pm 0.59 \pm 0.47$
0.42–0.50	0.457	44.7	$13.14 \pm 0.48 \pm 0.45$	0.458	54.6	$8.92 \pm 0.38 \pm 0.32$
0.50–0.60	0.544	44.5	$8.67 \pm 0.33 \pm 0.37$	0.544	54.5	$5.77 \pm 0.27 \pm 0.34$
0.60–0.72	0.656	44.6	$4.57 \pm 0.21 \pm 0.29$	0.653	54.4	$3.28 \pm 0.18 \pm 0.22$
0.72–0.90	0.789	44.9	$1.66 \pm 0.09 \pm 0.16$	0.790	54.6	$1.38 \pm 0.09 \pm 0.14$
0.90–1.25				1.016	54.2	$0.22 \pm 0.02 \pm 0.03$
p_T	$60 < \theta < 75$			$75 < \theta < 90$		
	$\langle p_\mathrm{T}\rangle$	$\langle\theta\rangle$	$\mathrm{d}^2\sigma/\mathrm{d}p\mathrm{d}\Omega$	$\langle p_\mathrm{T}\rangle$	$\langle\theta\rangle$	$\mathrm{d}^2\sigma/\mathrm{d}p\mathrm{d}\Omega$
0.13–0.16	0.146	67.2	$13.44 \pm 0.66 \pm 0.80$	0.145	82.6	$11.17 \pm 0.62 \pm 0.74$
0.16–0.20	0.180	67.2	$16.66 \pm 0.63 \pm 0.82$	0.180	82.2	$12.06 \pm 0.52 \pm 0.58$
0.20–0.24	0.220	66.9	$15.91 \pm 0.63 \pm 0.61$	0.219	82.3	$11.14 \pm 0.50 \pm 0.46$
0.24–0.30	0.269	67.2	$13.82 \pm 0.47 \pm 0.45$	0.269	82.0	$8.48 \pm 0.35 \pm 0.28$
0.30–0.36	0.329	67.2	$10.10 \pm 0.39 \pm 0.31$	0.330	81.6	$6.09 \pm 0.30 \pm 0.22$
0.36–0.42	0.390	66.7	$7.17 \pm 0.32 \pm 0.26$	0.389	82.0	$4.01 \pm 0.24 \pm 0.18$
0.42–0.50	0.457	66.8	$5.45 \pm 0.24 \pm 0.23$	0.457	81.5	$3.30 \pm 0.19 \pm 0.17$
0.50–0.60	0.545	66.5	$3.04 \pm 0.15 \pm 0.17$	0.544	81.7	$1.70 \pm 0.12 \pm 0.12$
0.60–0.72	0.653	66.9	$1.82 \pm 0.11 \pm 0.14$	0.655	81.4	$0.95 \pm 0.09 \pm 0.08$
0.72–0.90	0.785	66.5	$0.65 \pm 0.05 \pm 0.07$	0.791	81.5	$0.28 \pm 0.03 \pm 0.04$
0.90–1.25	1.018	65.1	$0.09 \pm 0.01 \pm 0.02$	1.006	81.2	$0.04 \pm 0.01 \pm 0.02$
p_T	$90 < \theta < 105$			$105 < \theta < 125$		
	$\langle p_\mathrm{T}\rangle$	$\langle\theta\rangle$	$\mathrm{d}^2\sigma/\mathrm{d}p\mathrm{d}\Omega$	$\langle p_\mathrm{T}\rangle$	$\langle\theta\rangle$	$\mathrm{d}^2\sigma/\mathrm{d}p\mathrm{d}\Omega$
0.13–0.16	0.146	97.4	$9.44 \pm 0.55 \pm 0.66$	0.145	114.3	$7.67 \pm 0.41 \pm 0.55$
0.16–0.20	0.180	97.2	$9.09 \pm 0.45 \pm 0.52$	0.179	114.2	$6.20 \pm 0.31 \pm 0.38$
0.20–0.24	0.219	97.4	$7.08 \pm 0.37 \pm 0.31$	0.218	114.0	$5.35 \pm 0.29 \pm 0.27$
0.24–0.30	0.269	97.1	$5.74 \pm 0.29 \pm 0.26$	0.269	113.6	$3.14 \pm 0.18 \pm 0.14$
0.30–0.36	0.328	96.9	$3.62 \pm 0.23 \pm 0.16$	0.327	113.6	$2.08 \pm 0.15 \pm 0.11$
0.36–0.42	0.388	96.6	$2.64 \pm 0.19 \pm 0.15$	0.387	112.0	$1.27 \pm 0.12 \pm 0.10$
0.42–0.50	0.459	97.1	$1.84 \pm 0.14 \pm 0.14$	0.456	113.1	$0.69 \pm 0.07 \pm 0.06$
0.50–0.60	0.544	96.9	$0.86 \pm 0.09 \pm 0.08$	0.536	113.0	$0.45 \pm 0.06 \pm 0.06$
0.60–0.72	0.649	95.8	$0.58 \pm 0.07 \pm 0.07$	0.652	111.7	$0.10 \pm 0.02 \pm 0.02$
0.72–0.90	0.796	96.9	$0.13 \pm 0.02 \pm 0.02$	0.768	112.2	$0.05 \pm 0.02 \pm 0.02$

Table 10 Double-differential inclusive cross-section $d^2\sigma/dpd\Omega$ [mb/(GeV/c sr)] of the production of π^-'s in $\pi^- + \text{Be} \to \pi^- + \text{X}$ interactions with -8.0 GeV/c beam momentum; the first error is statistical, the second systematic; p_T in GeV/c, polar angle θ in degrees

p_T	$20 < \theta < 30$			$30 < \theta < 40$		
	$\langle p_T \rangle$	$\langle \theta \rangle$	$d^2\sigma/dpd\Omega$	$\langle p_T \rangle$	$\langle \theta \rangle$	$d^2\sigma/dpd\Omega$
0.10–0.13	0.116	24.8	$62.88 \pm 2.02 \pm 4.24$	0.116	34.8	$41.80 \pm 1.61 \pm 2.90$
0.13–0.16	0.145	24.6	$85.27 \pm 2.21 \pm 4.78$	0.145	34.5	$53.90 \pm 1.73 \pm 2.88$
0.16–0.20	0.180	24.6	$95.38 \pm 1.93 \pm 4.18$	0.181	34.7	$63.73 \pm 1.57 \pm 2.83$
0.20–0.24	0.220	24.7	$97.33 \pm 1.93 \pm 3.65$	0.220	34.7	$67.33 \pm 1.59 \pm 2.57$
0.24–0.30	0.269	24.7	$96.82 \pm 1.56 \pm 3.05$	0.269	34.6	$62.27 \pm 1.23 \pm 1.98$
0.30–0.36	0.329	24.8	$83.57 \pm 1.45 \pm 2.36$	0.329	34.5	$52.83 \pm 1.12 \pm 1.49$
0.36–0.42	0.389	24.8	$67.94 \pm 1.30 \pm 2.05$	0.388	34.7	$43.38 \pm 1.03 \pm 1.23$
0.42–0.50	0.458	24.7	$55.32 \pm 1.01 \pm 1.86$	0.458	34.7	$34.45 \pm 0.79 \pm 1.12$
0.50–0.60	0.547	24.5	$34.34 \pm 0.71 \pm 1.53$	0.545	34.6	$23.14 \pm 0.58 \pm 0.98$
0.60–0.72	0.654	24.4	$21.28 \pm 0.51 \pm 1.26$	0.655	34.8	$12.91 \pm 0.39 \pm 0.75$
0.72–0.90				0.799	34.9	$5.46 \pm 0.20 \pm 0.44$
p_T	$40 < \theta < 50$			$50 < \theta < 60$		
	$\langle p_T \rangle$	$\langle \theta \rangle$	$d^2\sigma/dpd\Omega$	$\langle p_T \rangle$	$\langle \theta \rangle$	$d^2\sigma/dpd\Omega$
0.10–0.13	0.115	44.9	$30.80 \pm 1.33 \pm 2.28$			
0.13–0.16	0.146	44.9	$39.52 \pm 1.44 \pm 2.16$	0.145	54.8	$28.11 \pm 1.18 \pm 1.73$
0.16–0.20	0.180	44.9	$46.83 \pm 1.34 \pm 2.11$	0.180	54.8	$33.93 \pm 1.13 \pm 1.54$
0.20–0.24	0.220	44.8	$47.27 \pm 1.35 \pm 1.83$	0.220	54.8	$31.77 \pm 1.08 \pm 1.21$
0.24–0.30	0.270	44.8	$42.06 \pm 1.01 \pm 1.35$	0.269	54.6	$30.99 \pm 0.87 \pm 0.99$
0.30–0.36	0.329	44.7	$34.59 \pm 0.90 \pm 0.99$	0.329	54.7	$25.41 \pm 0.78 \pm 0.75$
0.36–0.42	0.389	44.9	$29.93 \pm 0.86 \pm 0.89$	0.389	54.6	$19.27 \pm 0.67 \pm 0.60$
0.42–0.50	0.458	44.7	$21.17 \pm 0.61 \pm 0.73$	0.458	54.7	$14.23 \pm 0.50 \pm 0.52$
0.50–0.60	0.547	44.7	$14.45 \pm 0.46 \pm 0.65$	0.546	54.6	$9.78 \pm 0.37 \pm 0.47$
0.60–0.72	0.656	44.6	$7.58 \pm 0.29 \pm 0.47$	0.654	54.6	$5.35 \pm 0.24 \pm 0.34$
0.72–0.90	0.794	44.4	$3.82 \pm 0.17 \pm 0.33$	0.793	54.7	$2.41 \pm 0.14 \pm 0.21$
0.90–1.25				1.023	54.2	$0.41 \pm 0.04 \pm 0.06$
p_T	$60 < \theta < 75$			$75 < \theta < 90$		
	$\langle p_T \rangle$	$\langle \theta \rangle$	$d^2\sigma/dpd\Omega$	$\langle p_T \rangle$	$\langle \theta \rangle$	$d^2\sigma/dpd\Omega$
0.13–0.16	0.146	67.3	$22.50 \pm 0.85 \pm 1.35$	0.146	82.6	$17.59 \pm 0.73 \pm 1.21$
0.16–0.20	0.180	67.3	$26.16 \pm 0.78 \pm 1.20$	0.179	82.4	$20.63 \pm 0.69 \pm 1.03$
0.20–0.24	0.219	67.0	$23.97 \pm 0.75 \pm 0.87$	0.219	82.0	$17.58 \pm 0.63 \pm 0.68$
0.24–0.30	0.268	67.0	$21.19 \pm 0.58 \pm 0.65$	0.268	81.8	$14.01 \pm 0.47 \pm 0.43$
0.30–0.36	0.329	66.8	$16.07 \pm 0.49 \pm 0.48$	0.328	81.9	$9.73 \pm 0.39 \pm 0.34$
0.36–0.42	0.389	67.0	$12.21 \pm 0.44 \pm 0.41$	0.388	82.2	$6.75 \pm 0.32 \pm 0.28$
0.42–0.50	0.456	66.8	$8.85 \pm 0.32 \pm 0.36$	0.457	81.6	$5.33 \pm 0.25 \pm 0.27$
0.50–0.60	0.545	66.9	$5.73 \pm 0.23 \pm 0.31$	0.544	81.9	$2.91 \pm 0.16 \pm 0.20$
0.60–0.72	0.655	66.8	$2.66 \pm 0.14 \pm 0.19$	0.650	81.6	$1.30 \pm 0.10 \pm 0.12$
0.72–0.90	0.793	66.4	$1.17 \pm 0.08 \pm 0.12$	0.779	81.1	$0.32 \pm 0.04 \pm 0.04$
0.90–1.25	1.006	66.4	$0.10 \pm 0.02 \pm 0.02$	1.042	79.8	$0.05 \pm 0.01 \pm 0.02$
p_T	$90 < \theta < 105$			$105 < \theta < 125$		
	$\langle p_T \rangle$	$\langle \theta \rangle$	$d^2\sigma/dpd\Omega$	$\langle p_T \rangle$	$\langle \theta \rangle$	$d^2\sigma/dpd\Omega$
0.13–0.16	0.145	97.2	$15.89 \pm 0.69 \pm 1.21$	0.146	114.8	$14.31 \pm 0.56 \pm 1.00$
0.16–0.20	0.180	97.4	$16.27 \pm 0.58 \pm 0.89$	0.179	114.3	$11.82 \pm 0.43 \pm 0.62$
0.20–0.24	0.219	97.3	$13.44 \pm 0.54 \pm 0.57$	0.218	114.3	$8.73 \pm 0.39 \pm 0.32$
0.24–0.30	0.267	96.8	$9.30 \pm 0.38 \pm 0.31$	0.267	114.0	$5.06 \pm 0.25 \pm 0.22$
0.30–0.36	0.327	97.0	$6.47 \pm 0.32 \pm 0.27$	0.329	113.9	$3.10 \pm 0.19 \pm 0.18$
0.36–0.42	0.389	96.9	$4.37 \pm 0.26 \pm 0.24$	0.389	113.5	$1.99 \pm 0.15 \pm 0.16$
0.42–0.50	0.456	96.4	$2.87 \pm 0.19 \pm 0.21$	0.454	111.9	$0.82 \pm 0.08 \pm 0.08$
0.50–0.60	0.545	95.9	$1.38 \pm 0.11 \pm 0.14$	0.541	112.4	$0.26 \pm 0.04 \pm 0.04$
0.60–0.72	0.655	96.3	$0.41 \pm 0.05 \pm 0.06$	0.646	110.0	$0.09 \pm 0.02 \pm 0.02$
0.72–0.90	0.790	96.8	$0.08 \pm 0.02 \pm 0.02$			

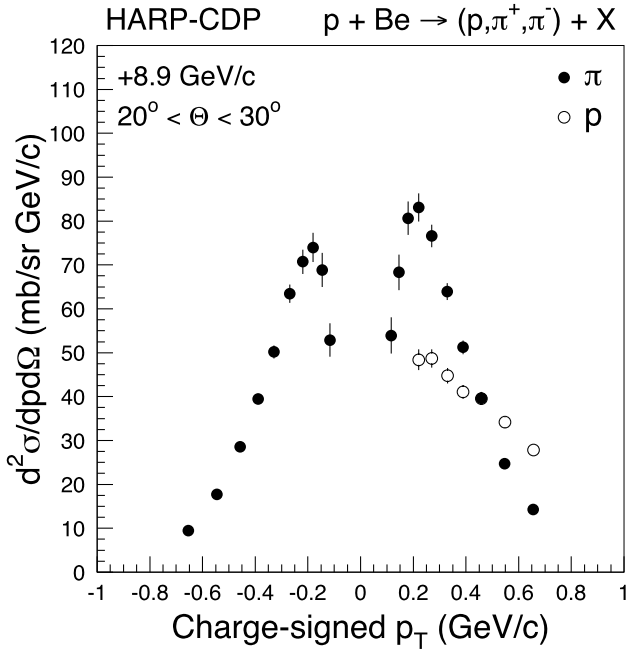

Fig. 13 Inclusive cross-sections as a function of charge-signed p_T of proton and $\pi^{\pm}$ production by +8.9 GeV/c incoming protons, off beryllium nuclei, in the polar-angle range $20° < \theta < 30°$

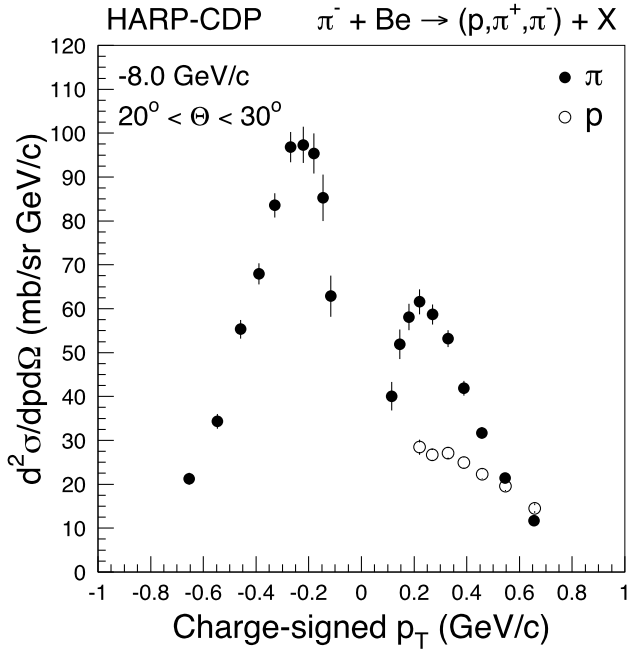

Fig. 15 Inclusive cross-sections as a function of charge-signed p_T of proton and $\pi^{\pm}$ production by -8.0 GeV/c incoming π^-'s, off beryllium nuclei, in the polar-angle range $20° < \theta < 30°$

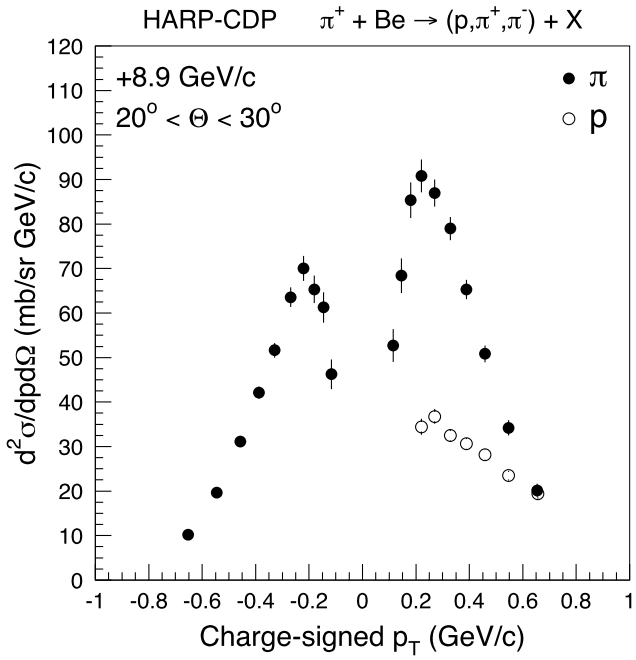

Fig. 14 Inclusive cross-sections as a function of charge-signed p_T of proton and $\pi^{\pm}$ production by +8.9 GeV/c incoming π^+'s, off beryllium nuclei, in the polar-angle range $20° < \theta < 30°$

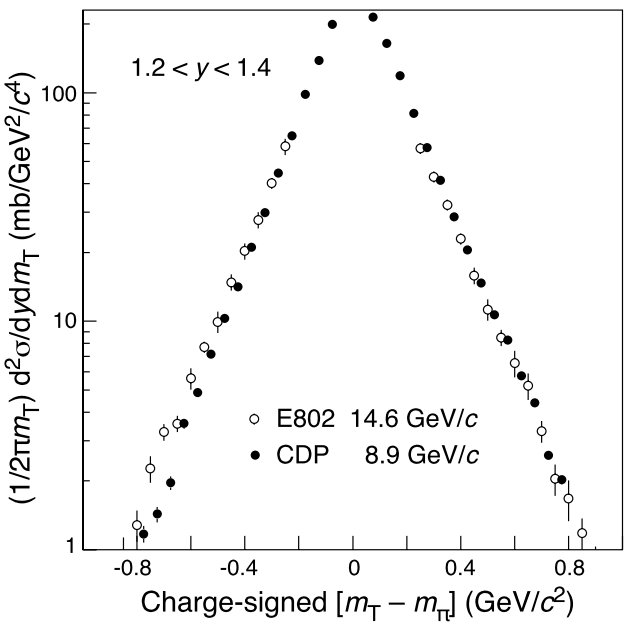

Fig. 16 Comparison of our cross-sections (*black circles*) of $\pi^{\pm}$ production by +8.9 GeV/c protons off beryllium nuclei, with the cross-sections published by the E802 Collaboration for the proton beam momentum of 14.6 GeV/c (*open circles*); the errors are statistical only

We note that both experiments agree in suggesting an exponential decrease of the invariant cross-section with increasing $m_T - m_\pi$, over two orders of magnitude. Unlike the π^- cross-sections, the π^+ cross-sections at +8.9 and +14.6 GeV/c exhibit nearly the same slope. In the comparison of absolute cross-sections, the E802 normalization un-

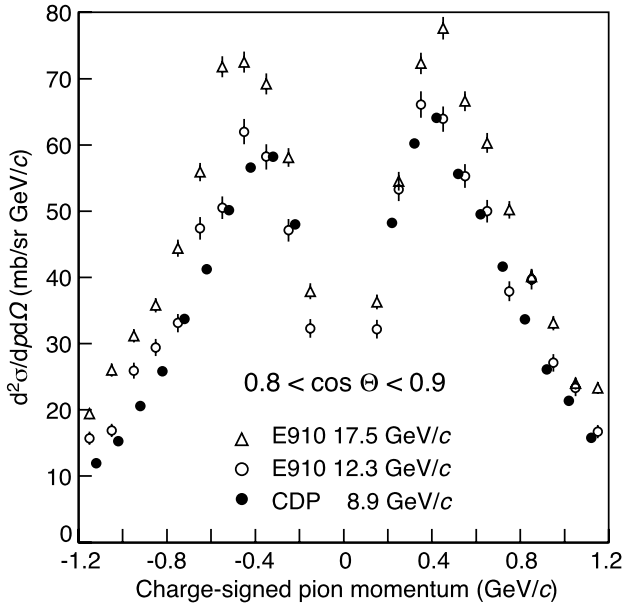

Fig. 17 Comparison of our cross-sections (*black circles*) of $\pi^{\pm}$ production by +8.9 GeV/*c* protons off beryllium nuclei with the cross-sections published by the E910 Collaboration for proton beam momenta of 12.3 (*open circles*) and 17.5 (*open triangles*) GeV/*c*; the errors are statistical only

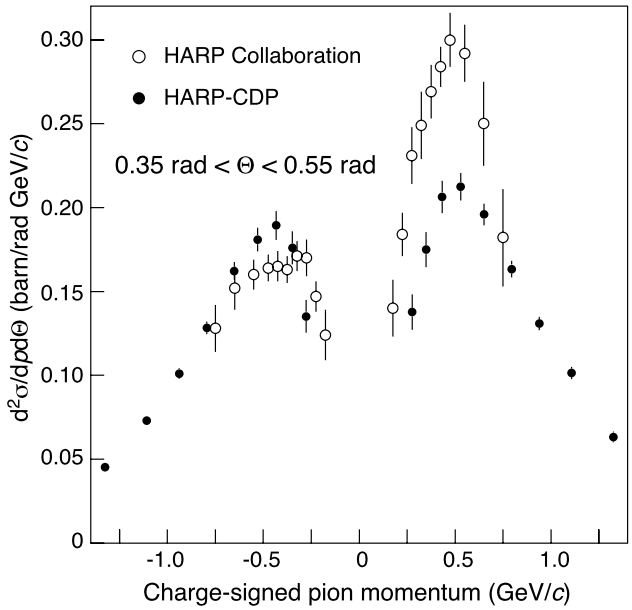

Fig. 18 Comparison of our cross-sections (*black circles*) of $\pi^{\pm}$ production by +8.9 GeV/*c* protons off beryllium nuclei with the cross-sections published by the HARP Collaboration (*open circles*)

certainty of (10–15)% is to be taken into account on top of the beam energy difference.

9.2 Comparison with E910 results

Experiment E910 [24] at Brookhaven National Laboratory measured secondary charged pions in the momentum range 0.1–6 GeV/*c* from the interactions of 12.3 and 17.5 GeV/*c* protons with beryllium nuclei. This experiment used a TPC for the measurement of secondaries, with a comfortably large track length of ∼1.5 m. With a magnetic field strength of 0.5 T, this large track length renders charge identification and proton–pion separation by $\mathrm{d}E/\mathrm{d}x$ beyond doubt.

Also here, the E910 data are shown as published, and our data are expressed in the same units as used by E910. Although the E910 measurements were made with proton beam momenta of 12.3 and 17.5 GeV/*c*, respectively, we note the similar π^+/π^- ratio between the cross-sections from E910 and our cross-sections from a proton beam momentum of 8.9 GeV/*c*, shown in Fig. 17. In the comparison of absolute cross-sections, the E910 normalization uncertainty of ≤5% is to be taken into account on top of the beam energy differences.

9.3 Comparison with results from the HARP Collaboration

Figure 18 shows the comparison of our cross-sections of pion production by +8.9 GeV/*c* protons off beryllium nuclei with the results published by the HARP Collaboration [25], in the polar-angle range $0.35 < \theta < 0.55$ rad. The latter cross-sections are plotted as published, while we expressed our cross-sections in the units used by the HARP Collaboration.

There is a severe discrepancy between our cross-sections and those reported by the HARP Collaboration. We note the difference especially of the π^+ cross-section, and the difference in the momentum range. The discrepancy is even more serious as the same data set has been analysed by both groups. For a discussion of the reasons for this discrepancy we refer to the Appendix of this paper.

10 Summary

From the analysis of data from the HARP large-angle spectrometer (polar angle θ in the range $20° < \theta < 125°$), double-differential cross-sections $\mathrm{d}^2\sigma/\mathrm{d}p\mathrm{d}\Omega$ of the production of secondary protons, π^+'s, and π^-'s, have been obtained. The incoming beam particles were +8.9 GeV/*c* protons and pions, and −8.0 GeV/*c* pions, impinging on a 5% λ_{abs} thick stationary beryllium target. The high statistics of the +8.9 GeV/*c* data allowed us to determine cross-sections of K^+ and deuteron production, albeit with lower precision. Our cross-sections for π^+ and π^- production agree with results from other experiments but disagree with the results of the HARP Collaboration that were obtained from the same raw data.

Acknowledgements We are greatly indebted to many technical collaborators whose diligent and hard work made the HARP detector a

well-functioning instrument. We thank all HARP colleagues who devoted time and effort to the design and construction of the detector, to data taking, and to setting up the computing and software infrastructure. We express our sincere gratitude to HARP's funding agencies for their support.

Appendix

The situation that two groups of authors, in this case the 'HARP Collaboration' (referred to as 'OH' for 'Official HARP') and us, the HARP-CDP group, publish inconsistent results from the same raw data, is unusual and unsatisfactory. Naturally, the question arises as to whose results can be trusted.

The central problem in OH's data analysis is their lack of understanding TPC track distortions which leads to:

- a bias of $\Delta(1/p_{\mathrm{T}}) \simeq 0.3\ (\mathrm{GeV}/c)^{-1}$ in their reconstruction of TPC tracks; in other words, their relative p_{T} bias increases linearly with p_{T} and attains some 30% at $p_{\mathrm{T}} = 1$ GeV/c; the bias is such that for particles with positive charge p_{T} is decreased, while for particles with negative charge p_{T} is increased;
- a resolution of $\sigma(1/p_{\mathrm{T}}) \simeq 0.6\ (\mathrm{GeV}/c)^{-1}$ which is considerably worse than $\sigma(1/p_{\mathrm{T}}) \simeq 0.30\ (\mathrm{GeV}/c)^{-1}$ claimed by OH; and
- a bad overall RPC time-of-flight resolution of 305 ps and an apparent advance of the timing signal of protons with respect to that of pions by ∼500 ps ('500 ps effect').

These three problems, together with a number of additional mistakes [26, 27], have the following fatal consequences for cross-sections of secondary hadron production:

- cross-section spectra of secondary hadrons are distorted especially in regions where cross-sections vary strongly with momentum; and
- protons and pions are partly confused.

Discussions of the flaws in the OH analysis have been published in [3] and [4]. Criticisms of the OH analysis by independent review bodies can be found in [9, 10]. We summarize here the main points.

OH's argument that 'dynamic' TPC track distortions can be neglected during the first third of the 400 ms long accelerator spill [8], reads as "*...owing to their limited mobility the first* [argon] *ions created in the amplification region need about 25 ms to reach the drift region and subsequently the steady flow of ions into this region only starts approximately 100 ms after the start of the spill, with a gradual transition between these two regimes...*" This argument is wrong. With an electric field strength of ∼1.7 kV/cm the argon ions need less than 1 ms for the relevant distance of 11 mm. Therefore, dynamic TPC track distortions increase right away approximately linearly with time in the spill. (Dynamic track distortions in the HARP TPC attain in the $r\cdot\phi$ coordinate ∼10 mm at the end of the spill, one order of magnitude larger than the typical $r\cdot\phi$ resolution; the correct algorithms to cope with TPC track distortions are described in [1] and in ample detail in [28–31].)

OH's claims in [8] that "*...The constrained fit* [which uses the beam point in addition to the TPC clusters] *is unbiased with respect to the unconstrained fit* [which uses the TPC clusters only]..." and "*...The weight of the vertex constraint compensates very well the distortions...*" contradict logic. It is impossible that a circle fit of TPC clusters that shifted away from their nominal $r\cdot\phi$ positions, together with the (undistorted) beam point, yields the same p_{T} as a fit of the distorted TPC clusters alone. It is equally impossible that a circle fit of the distorted TPC clusters together with the undistorted beam point gives an unbiased p_{T} estimate.

OH's justification of their claim of the absence of a bias in their circle fit stems from Fig. 4 in [8]: "*...In Fig. 4 it is shown that the vertex constraint does not introduce biases for those particle trajectories and that the simulation provides an excellent description of the behaviour of the resolution function...*". Their Fig. 4 claims to prove the equality of momentum from OH's 'constrained' and 'unconstrained fits'. That this claim is wrong is evident from the unphysical non-Gaussian shape of the shown distribution. Its cause is a mistake in their calculation of the $r\cdot\phi$ error of TPC clusters: their $\sigma^2_{r\phi}$ is multiplied by a factor $\cos^2 2\phi$ which assigns clusters an unphysically large weight depending on how close they are to the singular values $\phi = 45°$, 135°, 225° and 315° in the azimuthal angle. (The mathematical intricacies of this mistake are explained in [26].)

OH never presented evidence that their p_{T} resolution during the accelerator spill is indeed $\sigma(1/p_{\mathrm{T}}) \simeq 0.30\ (\mathrm{GeV}/c)^{-1}$, and that after TPC track distortion corrections their $r\cdot\phi$ residuals with respect to an unbiased external coordinated system are compatible with zero across the whole active TPC volume.

In their most recent physics publication [25], OH claim "*...Corrections that allow use of the full statistics to be made, correcting for such* [dynamic] *distortions, have been developed... and are fully applied in this analysis. The obtained results are fully compatible within the statistical errors and differential systematic uncertainties with those previously published...*". This claimed agreement between data from the first third of the spill without distortion correction, with data from the full spill with distortion correction, permits the conclusion that OH's full-spill analysis is beset by the same flaws as their earlier analysis of data from the first third of the spill.

Since OH have a biased track momentum, they observe that the RPC timing signal of protons is advanced with respect to the RPC timing signal of (relativistic) pions. This '500 ps effect' observation led them to conclude in [35]

"*...While this is in itself an interesting effect ...it prevents the use of the RPCs as a method to verify the reconstructed momentum scale of heavily ionizing particles* [protons]." As a consequence, they made no use of the powerful particle identification capability from RPC time of flight. The exclusive use of $\mathrm{d}E/\mathrm{d}x$ from the TPC in conjunction with a biased track momentum leads to the partial confusion of protons and pions in OH's analysis.

OH's interpretation of the '500 ps effect' is characterized by statements like "*...One possible explanation is the fluctuation in arrival time of the first cluster of the primary ionization. This fluctuation is smaller for heavily ionizing particles* [protons]..." in [7], or "*...An order of magnitude estimate of the effect given the propagation velocity of electrons in the gas and the chamber gap leads to an order of magnitude of a few 100 ps...*" in [35]. This understanding of signal generation is wrong. The anode signal is generated by induction. Hence the (fast) propagation of electromagnetic waves across the gas gap is relevant and not the arrival at the anode of—in comparison—slowly moving electrons. (The correct mechanism of RPC-signal generation is described in [2].)

We conclude that claims and results published by OH [5–8, 25, 32–34, 36–38] suffer from systematic biases and shortcomings that are absent in our analyses presented in this and forthcoming papers.

References

1. V. Ammosov et al., Nucl. Instrum. Methods Phys. Res. A **588**, 294 (2008)
2. V. Ammosov et al., Nucl. Instrum. Methods Phys. Res. A **578**, 119 (2007)
3. V. Ammosov et al., J. Instrum. **3**, P01002 (2008)
4. V. Ammosov et al., Eur. Phys. J. C **54**, 169 (2008)
5. M.G. Catanesi et al., Nucl. Instrum. Methods Phys. Res. A **571**, 527 (2007)
6. M. Bogomilov et al., IEEE Trans. Nucl. Sci. **54**, 342 (2007)
7. A. Artamonov et al., J. Instrum. **2**, P10004 (2007)
8. M.G. Catanesi et al., J. Instrum. **3**, P04007 (2008)
9. Report on HARP Data comparisons, CERN-SPSC-2009-004 (SPSC-M-768)
10. Minutes of the SPSC Meetings, http://cern.ch/Committees/SPSC/datesSPSCminutes.html
11. V. Ammosov et al., CERN-HARP-CDP-2008-001 (HARP Memo 08-101)
12. V. Ammosov et al., CERN-HARP-CDP-2008-002 (HARP Memo 08-102)
13. K. Fujii et al., Nucl. Instrum. Methods Phys. Res. A **264**, 297 (1988)
14. F. Dydak, Yu. Nefedov, CERN-HARP-CDP-2004-001 (HARP Memo 04-002)
15. K. Fujii et al., Track reconstruction with the TRISTAN-TOPAZ TPC, KEK preprint 87-24; JLC Physics Group, Introduction to helical track manipulations (Internal Report, 6 June 1997)
16. V. Ammosov et al., CERN-HARP-CDP-2006-005 (HARP Memo 06-103)
17. N.I. Chernov, G.A. Ososkov, Comput. Phys. Commun. **33**, 329 (1984)
18. S. Agostinelli et al., Nucl. Instrum. Methods Phys. Res. A **506**, 250 (2003)
19. J. Allison et al., IEEE Trans. Nucl. Sci. **53**, 270 (2006)
20. A. Bolshakova et al., Eur. Phys. J. C **56**, 323 (2008)
21. A. Bolshakova et al., Tables of cross-sections of large-angle hadron production in proton- and pion-nucleus interactions I: beryllium nuclei and beam momenta of $+8.9$ GeV/c and -8.0 GeV/c, CERN-HARP-CDP-2009-001
22. A. Bolshakova et al., Cross-sections of large-angle hadron production in proton- and pion-nucleus interactions II: beryllium nuclei and beam momenta from ± 3 GeV/c to ± 15 GeV/c. Eur. Phys. J. C (2009, submitted)
23. T. Abbott et al., Phys. Rev. D **45**, 3906 (1992)
24. I. Chemakin et al., Phys. Rev. C **65**, 024904 (2002)
25. M.G. Catanesi et al., Phys. Rev. C **77**, 055207 (2008)
26. V. Ammosov et al., CERN-HARP-CDP-2006-003 (HARP Memo 06-101)
27. V. Ammosov et al., CERN-HARP-CDP-2006-007 (HARP Memo 06-105) and CERN-HARP-CDP-2007-001 (HARP Memo 07-101)
28. F. Dydak, CERN-HARP-CDP-2003-001 (HARP Memo 03-001)
29. F. Dydak, A. Krasnoperov, Yu. Nefedov, CERN-HARP-CDP-2003-002 (HARP Memo 03-002)
30. I. Boyko et al., CERN-HARP-CDP-2005-001 (HARP Memo 05-101)
31. V. Ammosov et al., CERN-HARP-CDP-2007-003 (HARP Memo 07-102)
32. M.G. Catanesi et al., Eur. Phys. J. C **51**, 787 (2007)
33. M.G. Catanesi et al., Eur. Phys. J. C **53**, 177 (2008)
34. M.G. Catanesi et al., Eur. Phys. J. C **54**, 37 (2008)
35. HARP Collaboration, arXiv:0709.2806v1 [physics.ins-det]
36. HARP Collaboration, Nucl. Instrum. Methods Phys. Res. A **571**, 564 (2007)
37. M. Bogomilov et al., IEEE Trans. Nucl. Sci. **54**, 1455 (2007)
38. HARP Collaboration, Nucl. Instrum. Methods Phys. Res. A **588**, 318 (2008)